Phosphatidylinositol 4-kinase IIα is a glycogen synthase kinase 3-regulated interaction hub for activity-dependent bulk endocytosis

Cell Reports

Article

Phosphatidylinositol 4-kinase IIα is a glycogen synthase kinase 3-regulated interaction hub for activity-dependent bulk endocytosis

Graphical abstract

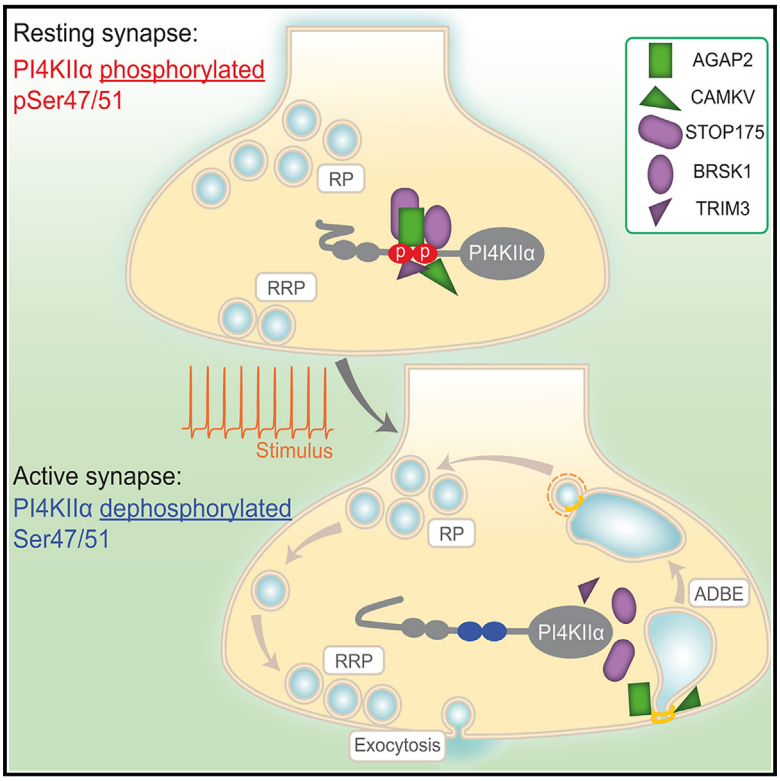

Highlights

- PI4KIIα is required for activity-dependent bulk endocytosis (ADBE)
- PI4KIIα phosphorylation is essential for this role, not its enzyme activity
- Phosphorylation at PI4KIIα Ser-47 causes binding of five presynaptic proteins
- Two of these interactors, AGAP2 and CAMKV, are essential for ADBE

Authors

Eva-Maria Blumrich, Jessica C. Nicholson-Fish, Marie Pronot, ..., Adam Cole, Karen J. Smillie, Michael A. Cousin

Correspondence

k.smillie@ed.ac.uk (K.J.S.), m.cousin@ed.ac.uk (M.A.C.)

In brief

Blumrich et al. reveal that phosphatidylinositol 4-kinase IIα (PI4KIIα) is required for activity-dependent bulk endocytosis (ADBE) at the presynapse. PI4KIIα acts as an interaction hub that liberates essential ADBE molecules, such as AGAP2 and CAMKV, via the activity-dependent control of its phosphorylation at key residues.

Blumrich et al., 2023, Cell Reports *42*, 112633
June 27, 2023
https://doi.org/10.1016/j.celrep.2023.112633

CellPress

Cell Reports

CellPress
OPEN ACCESS

Article

Phosphatidylinositol 4-kinase IIα is a glycogen synthase kinase 3-regulated interaction hub for activity-dependent bulk endocytosis

Eva-Maria Blumrich,[1,2,3] Jessica C. Nicholson-Fish,[1] Marie Pronot,[1,2,3] Elizabeth C. Davenport,[1,2,3] Dominic Kurian,[4] Adam Cole,[5] Karen J. Smillie,[1,2,*] and Michael A. Cousin[1,2,3,6,*]

[1]Centre for Discovery Brain Sciences, University of Edinburgh, Hugh Robson Building, George Square, Edinburgh, Scotland EH8 9XD, UK
[2]Muir Maxwell Epilepsy Centre, University of Edinburgh, Hugh Robson Building, George Square, Edinburgh, Scotland EH8 9XD, UK
[3]Simons Initiative for the Developing Brain, University of Edinburgh, Hugh Robson Building, George Square, Edinburgh, Scotland EH8 9XD, UK
[4]The Roslin Institute, University of Edinburgh, Easter Bush, Midlothian, Scotland EH25 9RG, UK
[5]Neurosignalling and Mood Disorders Group, The Garvan Institute of Medical Research, 384 Victoria Street, Darlinghurst, NSW 2010, Australia
[6]Lead contact
*Correspondence: k.smillie@ed.ac.uk (K.J.S.), m.cousin@ed.ac.uk (M.A.C.)
https://doi.org/10.1016/j.celrep.2023.112633

SUMMARY

Phosphatidylinositol 4-kinase IIα (PI4KIIα) generates essential phospholipids and is a cargo for endosomal adaptor proteins. Activity-dependent bulk endocytosis (ADBE) is the dominant synaptic vesicle endocytosis mode during high neuronal activity and is sustained by glycogen synthase kinase 3β (GSK3β) activity. We reveal the GSK3β substrate PI4KIIα is essential for ADBE via its depletion in primary neuronal cultures. Kinase-dead PI4KIIα rescues ADBE in these neurons but not a phosphomimetic form mutated at the GSK3β site, Ser-47. Ser-47 phosphomimetic peptides inhibit ADBE in a dominant-negative manner, confirming that Ser-47 phosphorylation is essential for ADBE. Phosphomimetic PI4KIIα interacts with a specific cohort of presynaptic molecules, two of which, AGAP2 and CAMKV, are also essential for ADBE when depleted in neurons. Thus, PI4KIIα is a GSK3β-dependent interaction hub that silos essential ADBE molecules for liberation during neuronal activity.

INTRODUCTION

Synaptic vesicle (SV) recycling is essential for the maintenance of neurotransmission. Central to this maintenance is the retrieval of SVs via different endocytosis modes that are triggered by specific patterns of neuronal activity in both time and space.[1,2] During sparse action potential trains, ultrafast endocytosis is dominant and generates small endosomal intermediates from which SVs are formed.[3] However, during elevated neuronal activity, this endocytosis mode saturates[4] and activity-dependent bulk endocytosis (ADBE) becomes the dominant SV regeneration mode.[5] Clathrin-mediated endocytosis (CME) acts to cluster SV cargo and generate SVs directly from these endosomes.[6,7]

During ADBE, large portions of the plasma membrane are engulfed, forming bulk endosomes.[5] These bulk endosomes are a platform for both the generation of new SVs for subsequent neurotransmitter release and trafficking carriers targeted to the endolysosomal system.[7–9] ADBE is coupled to neuronal activity via the calcium-dependent protein phosphatase calcineurin,[10–14] which dephosphorylates a series of endocytosis proteins to drive formation of bulk endosomes.[15] Glycogen synthase kinase 3β (GSK3β) sustains ADBE during repetitive activity by rephosphorylating some of these proteins, including the essential GTPase dynamin-1.[16] GSK3β is constitutively active and is inhibited by the same activity patterns that trigger ADBE,[17,18] suggesting that GSK3β coordinates ADBE via multiple presynaptic phosphorylation events.

Phosphatidylinositol (PI) phosphates perform critical roles in the SV life cycle.[19] The best characterized example of this is $PI(4,5)P_2$, which is essential for SV fusion,[20,21] CME,[22] and potentially ADBE.[23] A key enzyme in the synthesis of presynaptic $PI(4,5)P_2$ is phosphatidylinositol 4-kinase IIα (PI4KIIα), which is enriched at synapses and is responsible for SV-localized PI4K activity.[24–27]

PI4KIIα has biological roles in addition to $PI(4,5)P_2$ synthesis. For example, PI4KIIα also generates PIs that recruit adaptor proteins to membranes and directly interacts with adaptor protein complexes themselves.[27–29] This makes PI4KIIα unusual in that it operates as a cargo while facilitating its own recruitment via its catalytic engagement with adaptor proteins.[30,31] Furthermore, PI4KIIα shares interactions with

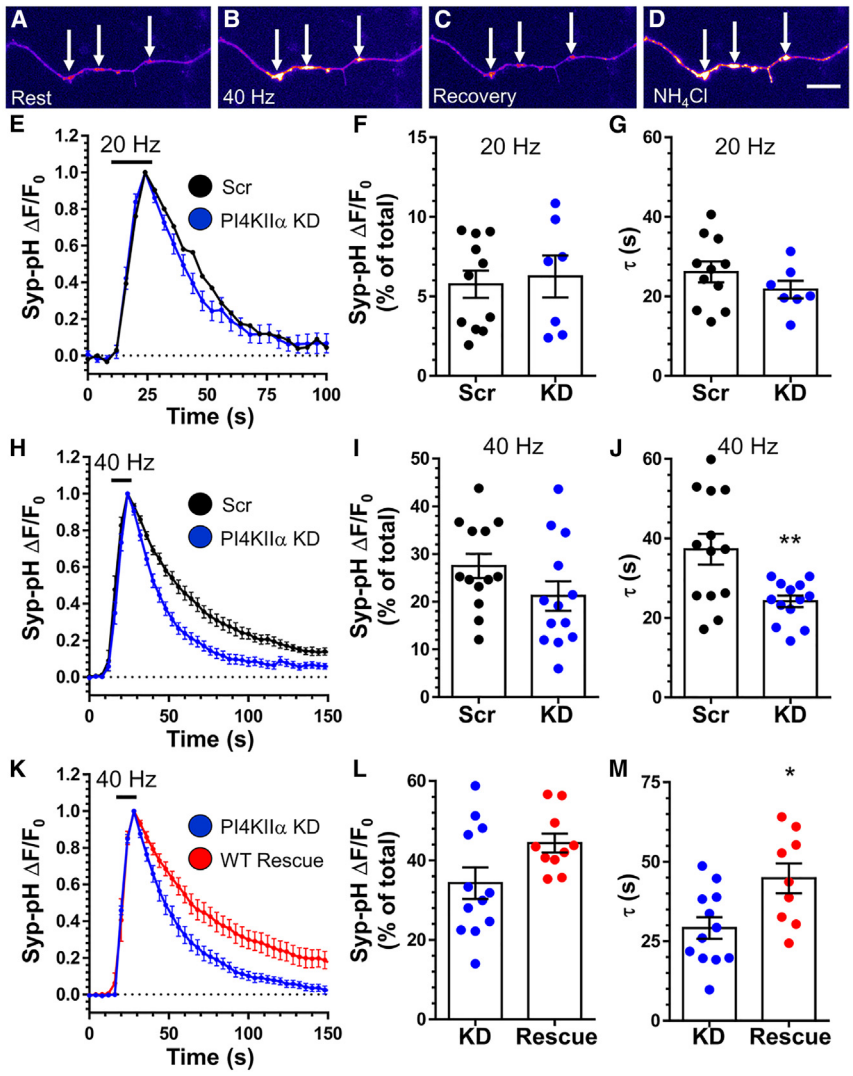

Figure 1. PI4KIIα retards SV endocytosis during high neuronal activity

(A–J) Primary cultures of CGNs were transfected with synaptophysin-pHluorin (syp-pH) and shRNA against either PI4KIIα (knockdown [KD]) or a scrambled (Scr) control between 5 and 7 days *in vitro* (DIV). At 8–10 DIV, CGNs were stimulated with a train of either 200 action potentials (20 Hz, E–G) or 400 action potentials (40 Hz, H–J). After 180 s, CGNs were pulsed with NH_4Cl imaging buffer. Representative images of the syp-pH response are displayed at rest (A), at 40 Hz (B), at recovery (C), and during NH_4Cl (D). Arrows indicate nerve terminals; scale bar: 10 μm. (E and H) Average fluorescent syp-pH response ($\Delta F/F_0 \pm$ SEM) normalized to the stimulation peak for either 20 (E) or 40 Hz (H) stimulation. (F and I) Peak syp-pH response to 20 (F) or 40 Hz (I) normalized to NH_4Cl ($\Delta F/F_0 \pm$ SEM). (G and J) Time constant (τ) of the syp-pH response to 20 (G) or 40 Hz (J) ± SEM. For 20 Hz, n = 11 Scr, n = 7 KD; 40 Hz, n = 13 for Scr and KD, **p = 0.004, unpaired t test.

(K–M) CGNs were transfected with syp-pH, PI4KIIα shRNA, and either FLAG-PI4KIIα (rescue) or an empty FLAG-tagged vector control (KD) between 5 and 7 DIV. CGNs were stimulated with action potentials (40 Hz, 10 s) and exposed to NH_4Cl as above. (K) Average fluorescent syp-pH response ($\Delta F/F_0 \pm$ SEM) normalized to stimulation peak. (L) Peak syp-pH response normalized to NH_4Cl ($\Delta F/F_0 \pm$ SEM). (M) Time constant (τ) of the syp-pH response ± SEM (n = 12 KD, n = 9 rescue, *p = 0.013, unpaired t test). In (E), (H), and (K), bar indicates period of stimulation.

components of the WASH complex, which generate localized domains for cargo sorting or membrane scission,[32] and the ubiquitin ligase Itch, which directs cargo to degradative sorting pathways.[33] Therefore, PI4KIIα has the potential to act as an interaction hub, with these interactions regulated by post-translational modifications.

PI4KIIα is phosphorylated on its N-terminal domain by GSK3β at two sites (Ser-5, Ser-47) after initial priming phosphorylation events at Ser-9 and Ser-51.[34] Given the links between ADBE, GSK3β, and the endolysosomal system,[7,16] we investigated the presynaptic role of PI4KIIα and its phosphorylation by GSK3β. We revealed that PI4KIIα is essential for ADBE and that this role requires the phosphorylation of Ser-47 by GSK3β. This phosphorylation event controls interactions with a cohort of presynaptic proteins, two of which, CAMKV and AGAP2, were discovered to be essential for ADBE. Therefore, PI4KIIα is a GSK3β-dependent interaction hub, which stockpiles distinct ADBE molecules for liberation during high neuronal activity.

RESULTS

PI4KIIα limits SV endocytosis kinetics during intense neuronal activity

PI4KIIα is highly expressed in brain and is enriched on SVs.[24–27] However, evidence for a direct role in mammalian SV recycling has relied on downstream analysis of its phospholipid end products, such as $PI(4,5)P_2$. To address the role of PI4KIIα directly, we first confirmed the presynaptic localization of PI4KIIα using immunofluorescence staining in primary cultures of cerebellar granule neurons (CGNs). PI4KIIα was highly expressed at the neuronal cell body, with a punctate distribution along axonal neurites (Figure S1). These PI4KIIα puncta corresponded to nerve terminals since a high degree of co-localization was observed with the SV protein synaptotagmin-1, similar to that of the SV protein SV2A (Figure S1). Thus, PI4KIIα is in the correct location to influence SV recycling.

We next determined whether loss of PI4KIIα had a direct impact on SV recycling by generating short hairpin RNA (shRNA) to deplete the endogenous enzyme in CGNs. PI4KIIα knockdown was highly efficient, with the endogenous enzyme reduced to approximately 25% of its level in non-transfected neurons (Figures S2A and S2B). SV recycling was monitored using the genetically encoded reporter synaptophysin-pHluorin (syp-pH).[35] Syp-pH is the SV protein synaptophysin with a pH-sensitive

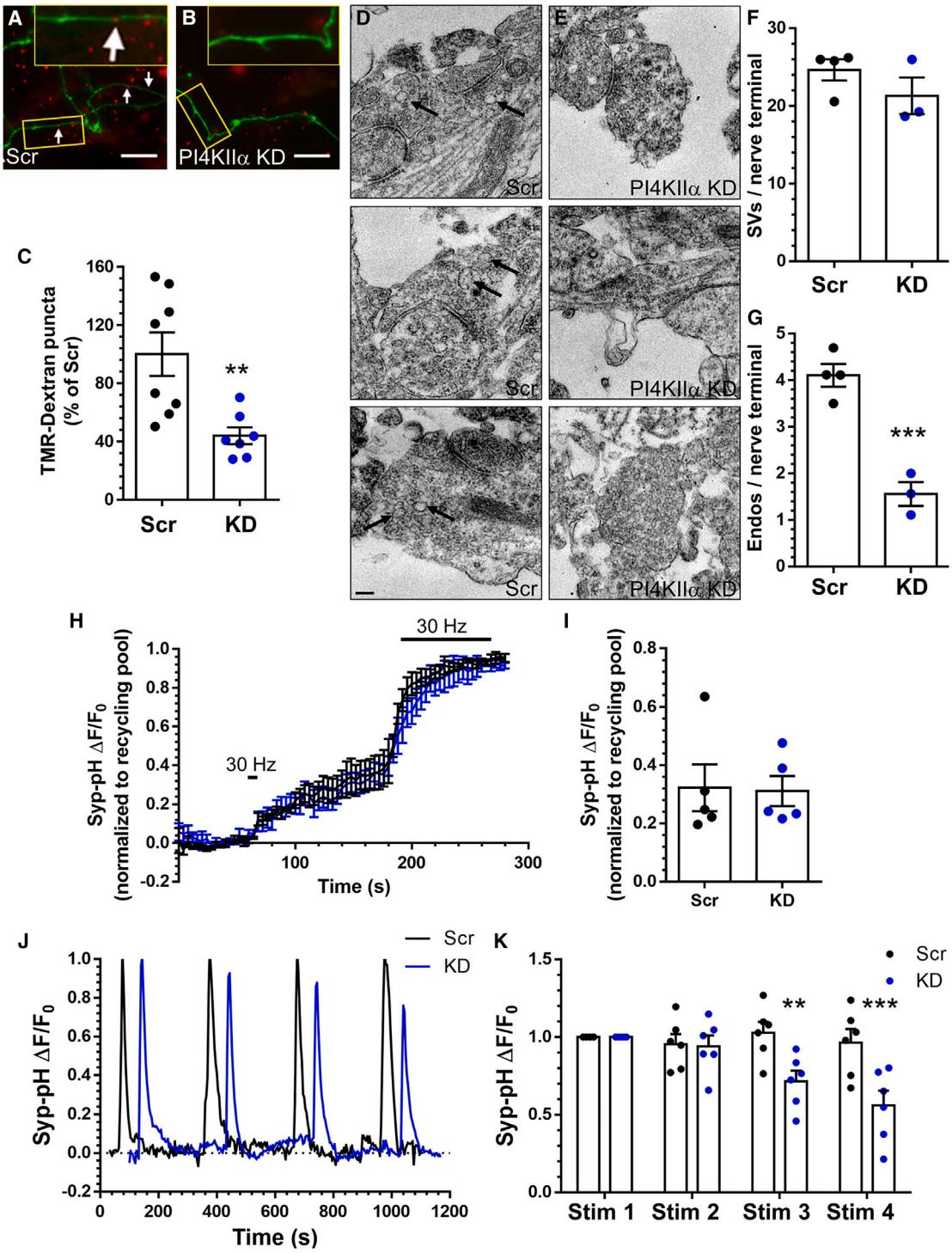

Figure 2. PI4KIIα controls ADBE via phosphorylation of GSK3 sites

(A–C) Primary cultures of CGNs were transfected with shRNA against either PI4KIIα (KD) or a Scr control between 5 and 7 DIV. At 8–10 DIV, CGNs were stimulated with a train of 400 action potentials (40 Hz) in the presence of 50 μM TMR-dextran for 2 min. (A and B) Representative images of TMR-dextran loading (red, arrow) in Scr (A) or KD (B) neurons (green), scale bar: 20 μm. (C) Mean TMR-dextran uptake as a proportion of total Scr uptake ± SEM (Scr n = 8, KD n = 7, **p = 0.0037, Mann-Whitney test).

(D–G) CGNs were transduced with lentivirus expressing either PI4KIIα shRNA (KD) or a Scr control at DIV 1. At 9 DIV, CGNs were stimulated with a train of 400 action potentials (40 Hz) and immediately fixed and processed for electron microscopy. (D and E) Representative images of CGN nerve terminals transduced with

(legend continued on next page)

GFP moiety fused to an intraluminal loop. Since the interior of the SV is acidic, SV exocytosis is visualized as an increase in fluorescence when the reporter is exposed to the extracellular medium (Figures 1A–1D). The kinetics and extent of SV endocytosis can also be determined by monitoring the decrease in fluorescence post-stimulation since SV endocytosis is rate limiting.[36,37] In neurons expressing scrambled shRNA, a characteristic syp-pH response was observed during stimulation with an action potential train (20 Hz, 10 s). This comprised an activity-dependent fluorescence increase and slow return to baseline (Figure 1E). Neurons that were depleted of PI4KIIα displayed a similar response (Figures 1E–1G). Thus, PI4KIIα performs no obvious role in SV recycling during moderate stimulation.

Latent molecular requirements for SV recycling can be revealed when the process is challenged with physiological stressors, such as during challenge with high intensity stimuli.[38,39] Therefore, we examined SV recycling in PI4KIIα-depleted neurons during stimulation with a train of high-frequency action potentials (40 Hz, 10 s; Figure 1H). Once again, no effect on the extent of SV fusion was observed in PI4KIIα-depleted neurons (Figure 1I). However, SV endocytosis was now accelerated when compared with neurons expressing scrambled shRNA (Figure 1J). To confirm that this acceleration was due to PI4KIIα depletion, a shRNA-resistant form of the enzyme was co-expressed in PI4KIIα knockdown neurons. Exogenous PI4KIIα restored SV endocytosis kinetics when compared with PI4KIIα-depleted neurons expressing an empty vector (Figures 1K–1M). Thus, PI4KIIα limits the speed of SV endocytosis but only during intense neuronal activity.

PI4KIIα is required for ADBE

ADBE is the dominant mode of SV endocytosis during patterns of intense physiological activity in dissociated neuronal culture[5] and intact neuronal circuits[40] and in response to environmental stimuli *in vivo*.[41] The activity-dependent requirement in SV endocytosis for PI4KIIα we observed using syp-pH led us to investigate a potential role for it in ADBE using uptake of the fluid phase marker, 40 kDa tetramethylrhodamine (TMR)-dextran. TMR-dextran is a selective ADBE marker due its size exclusion from single SVs undergoing endocytosis.[5] Application of TMR-dextran during action potential stimulation (40 Hz, 10 s) resulted in distinct fluorescent puncta decorated along the axon of CGNs expressing scrambled shRNA, indicating triggering of ADBE (Figure 2A). TMR-dextran puncta were also observed in CGNs where PI4KIIα was depleted (Figure 2B); however, this number was reduced by greater than 50% when compared with scrambled shRNA controls (Figure 2C). Therefore, PI4KIIα is required for efficient ADBE during intense neuronal activity.

To confirm the requirement for PI4KIIα in ADBE, we performed morphological analysis of CGN nerve terminals transduced with shRNA against PI4KIIα or scrambled control shRNA (Figures S2C and S2D). CGNs were stimulated with an action potential train as above and then immediately fixed and processed for electron microscopy. There was no difference in the number of SVs after stimulation when PI4KIIα-depleted nerve terminals were compared with scrambled controls (Figures 2D–2F). However, there was a significant reduction in presynaptic endosomes (Figures 2D, 2E, and 2G). Therefore, two independent assays of ADBE reveal a key requirement for PI4KIIα in this endocytosis mode.

We next determined whether the reduction in ADBE in PI4KIIα-depleted neurons translated into observable dysfunction in neurotransmission. To achieve this, we utilized syp-pH as a surrogate of neurotransmitter release using established assays that determine either release probability (Pr) or synaptic depression. To investigate Pr, CGNs were challenged with a test pulse of 60 action potentials (30 Hz) to mobilize the readily releasable pool (RRP) followed by a saturating stimulus of 1,350 action potentials (30 Hz) to fuse the remaining SVs in the recycling pool. Experiments were performed in the presence of bafilomycin A1, which inhibits the V-type ATPase on SVs, to reveal SV fusion events in isolation.[42] An alteration in the size of the RRP response as a proportion of the larger recycling pool would therefore be indicative of a change in Pr.[7,43] When this experiment was performed, there was no significant difference in the size of the RRP when PI4KIIα-depleted neurons were compared with neurons expressing scrambled shRNA (Figures 2H and 2I). Therefore, PI4KIIα has no direct effect on the fusion competence of SVs.

While PI4KIIα may have no direct role in determining Pr, it may still modulate neurotransmission. This is because neurotransmitter release is sustained by the efficient endocytosis and recycling of SVs, and therefore inhibition of ADBE would be predicted to reduce SV fusion events during periods of repeated activity. This has been observed in neurons lacking either VAMP4 or fragile X messenger ribonucleoprotein (the absence of either results in a reduction in ADBE[44,45]). To determine the impact of reduced ADBE on the ability of neurons to sustain neurotransmission, CGNs expressing syp-pH and either PI4KIIα shRNA or a scrambled control were challenged with four high-frequency action potential trains (40 Hz, 10 s) at 5 min intervals. CGNs expressing scrambled shRNA were able to sustain equivalent syp-pH responses during repeated trains of stimuli (Figures 2J and 2K). In contrast, the syp-pH response in PI4KIIα-depleted CGNs was significantly lower by the third and fourth stimulus trains (Figures 2J and 2K). Therefore the reduction in ADBE observed in PI4KIIα-depleted CGNs translates into a drop in presynaptic performance.

either Scr (D) or KD (E). Presynaptic endosomes indicated by arrows, scale bar: 150 nm. Mean number of SVs (F) and endosomes (G) per nerve terminal ± SEM (Scr n = 4, KD n = 3, F p = 0.2452, G ***p = 0.0009, unpaired t test).

(H–K) Primary cultures of CGNs were transfected with syp-pH and either PI4KIIα KD or Scr shRNA between 5 and 7 DIV, with experiments performed at 8–10 DIV. (H and I) CGNs were incubated with 1 μM bafilomycin A1 for 1 min and then stimulated with a train of 60 action potentials (30 Hz) followed by a second train of 30 Hz (45 s) 1 min later, stimulation indicated by bars. (H) Average fluorescent syp-pH response ($\Delta F/F_0$ ± SEM) normalized to the recycling pool (plateau after second stimulus). (I) Quantification of RRP size ± SEM (n = 5 for Scr and KD, p = 0.901, Student's t test). (J and K) CGNs were challenged with 4 trains of 400 action potential stimulation (40 Hz) at 5 min intervals. (J) Representative traces of the syp-pH response ($\Delta F/F_0$) normalized to the first stimulus. (K) Quantification of the syp-pH response ($\Delta F/F_0$ ± SEM) normalized to the first stimulus (n = 6 for Scr and KD, two-way ANOVA p = 0.0057; **p = 0075, ***p = 0.0004).

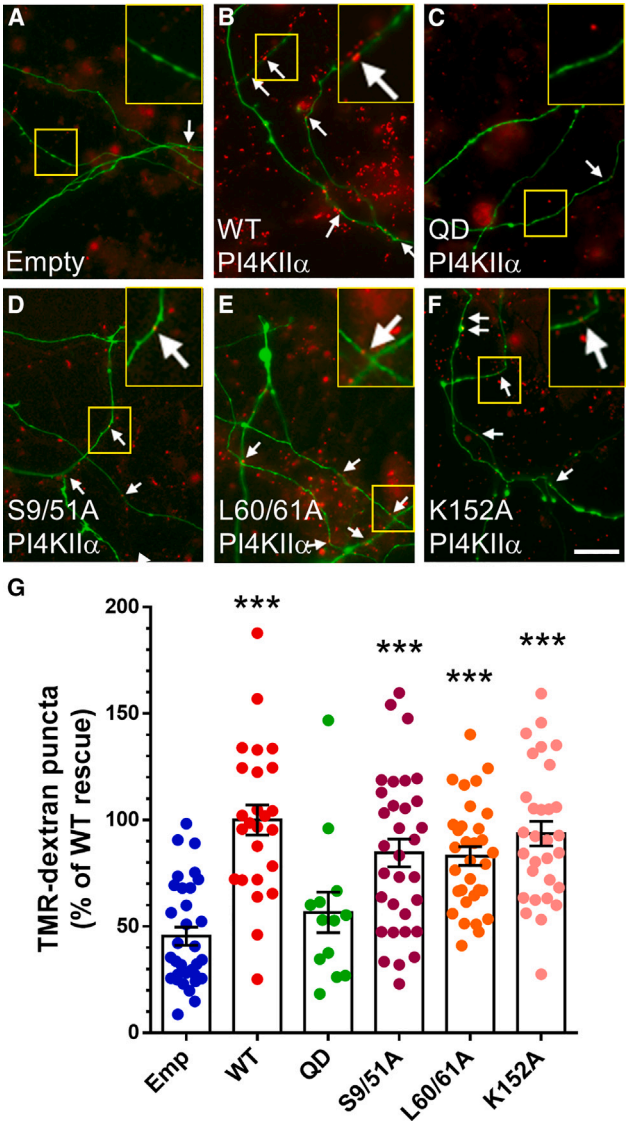

Figure 3. The phosphomimetic QD PI4KIIα mutant cannot correct ADBE in PI4KIIα-depleted CGNs

CGNs were transfected with PI4KIIα shRNA and either FLAG-tagged versions of PI4KIIα (WT), PI4KIIα-QD, PI4KIIα-S9/51A, PI4KIIα-L60/61A, PI4KIIα-K152A, or an empty FLAG vector (Emp) between 5 and 7 DIV. At 8–10 DIV, CGNs were stimulated with a train of 400 action potentials (40 Hz) in the presence of 50 μM TMR-dextran for 2 min.

(A–F) Representative images of TMR-dextran loading (red, arrows) in transfected neurons (green), scale bar: 20 μm.

(G) Mean TMR-dextran uptake as a proportion of uptake in WT expressing CGNs ± SEM (Emp, S9/51A, L60/61A n = 32, K152A n = 30, WT n = 25, QD n = 13, ****p < 0.0001, one-way ANOVA against Emp).

Phosphorylation of PI4KIIα controls ADBE

To determine the mechanism underpinning the requirement for PI4KIIα in ADBE, we performed molecular replacement experiments by co-expressing shRNA-resistant constructs designed to ablate specific interactions or functions of PI4KIIα (Figures 3A–3F). All of these mutants restored PI4KIIα expression to levels between 150% and 200% of endogenous enzyme (Figure S2B). Expression of exogenous wild-type PI4KIIα fully rescued ADBE, confirming its role in this endocytosis mode (Figure 3G). Interestingly, a kinase-dead mutant of PI4KIIα (K152A[46]) fully restored TMR-dextran uptake (Figure 3G), suggesting that the lipid kinase activity of this enzyme is dispensable for ADBE. To confirm the absence of a requirement for the lipid kinase activity of PI4KIIα, the effect of the selective antagonist PI273[47] on evoked TMR-dextran uptake was investigated. A 48 h incubation with 1 μM PI273 had no effect on activity-dependent (40 Hz, 10 s) TMR-dextran uptake when compared with a vehicle control (Figure S3A). Therefore, the lipid kinase activity of PI4KIIα is dispensable for ADBE.

The ability of kinase-dead PI4KIIα to correct ADBE in knockdown CGNs suggested that the enzyme may control this endocytosis mode via its interactions rather than its catalytic activity. Importantly, PI4KIIα is a GSK3β substrate, the activity of which is essential to sustain ADBE during trains of neuronal activity.[16] Furthermore, phosphorylation of PI4KIIα by GSK3β "opens" the PI4KIIα N terminus, permitting the binding of adaptor proteins at a di-leucine motif adjacent to the phosphorylation sites.[34] Therefore, we next determined the role of GSK3β-dependent phosphorylation of PI4KIIα in the control of ADBE. Importantly, since priming phosphorylation is essential for GSK3 phosphorylation to occur, the sites Ser-47/51 and Ser-5/9 will always share the same phosphorylation status. We first expressed either PI4KIIα, which cannot be phosphorylated by GSK3β (due to removal of its priming sites, S9/51A), or PI4KIIα, with a disrupted adaptor protein-binding motif (L60/61A). Both of these shRNA-resistant mutants fully restored TMR-dextran uptake to levels observed with wild-type PI4KIIα (Figure 3G). This indicates that phosphorylation-dependent interactions of PI4KIIα with classical adaptor protein complexes are not required for ADBE. However, expression of a mutant that mimicked GSK3β-phosphorylated PI4KIIα (S5/9/47/51D, QUAD-D [QD]) failed to restore ADBE in PI4KIIα-depleted CGNs, with similar levels of TMR-dextran uptake observed in CGNs where no rescue construct was expressed (empty vector control; Figure 3G). The inability of PI4KIIα-QD to restore ADBE in PI4KIIα-depleted cells may be due to disruption of its trafficking, resulting in a mislocalization from nerve terminals. However, PI4KIIα-QD displayed an identical subcellular distribution to that of PI4KIIα-WT at both the TGN and nerve terminals (Figure S3B). Therefore, mock phosphorylation of PI4KIIα at GSK3β-specific sites result in a loss of its functional role in ADBE.

To determine whether the inability of PI4KIIα-QD to restore ADBE was due to dominant-negative effects, it was overexpressed in CGNs that had not been depleted of PI4KIIα. PI4KIIα-QD expression did not affect activity-dependent TMR-dextran uptake in this instance, confirming that this was a loss-of-function mutant (Figure S3C). The expression of all other PI4KIIα mutants also had no impact of activity-dependent TMR-dextran uptake (Figure S3C). Therefore, GSK3β-dependent phosphorylation of PI4KIIα restricts its role in ADBE.

Phosphorylation of PI4KIIα controls ADBE via a specific subset of protein interactions

The inability of PI4KIIα-QD to correct TMR-dextran uptake in PI4KIIα knockdown neurons, combined with the absence of a

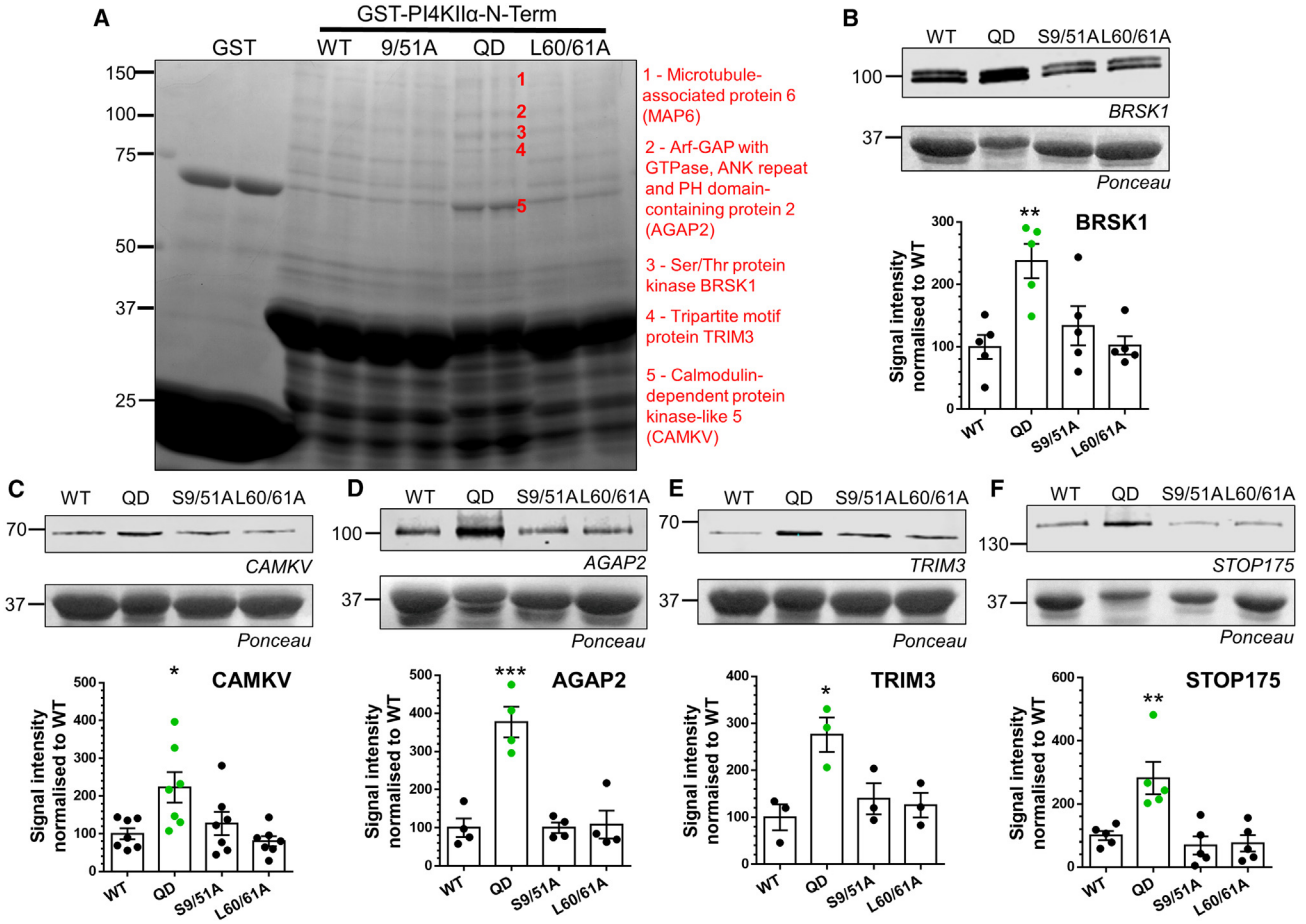

Figure 4. The QD PI4KIIα mutant interacts with a specific cohort of presynaptic proteins

PI4KIIα GST-fusion proteins generated from the wild-type (WT) PI4KIIα N terminus or a mutant version (QD, S9/51A, or L60/61A) were incubated with nerve terminal lysates with extracted proteins separated by SDS-PAGE and identified by mass spectrometry.

(A) Image of SDS-PAGE gel with 5 specific bands extracted by QD GST-PI4KIIα highlighted with their identities revealed to the right of the gel.

(B–F) Representative western blots of BRSK1 (B), CAMKV (C), AGAP2 (D), TRIM3 (E), and STOP175 (F) with their respective GST fusion proteins (Ponceau) are displayed in addition to quantification of their binding to WT, QD, S9/51A, and L60/61A GST-PI4KIIα ± SEM (CAMKV n = 7, BRSK1, STOP175 n = 5, AGAP2 n = 4, TRIM3 n = 3, ***p < 0.001, **p < 0.01, *p < 0.05, one-way ANOVA with Dunnett's multiple comparison test against WT).

role for its lipid kinase activity, suggests that PI4KIIα phosphorylation controls a protein interaction required for ADBE. To determine which interactions were modulated by phosphorylation, we generated GST-fusion proteins from the PI4KIIα N terminus (GST-PI4KIIα-N-term) with identical mutations to those used in the TMR-dextran assay (Figure 3). Interaction partners were then extracted from nerve terminal lysates by affinity purification and separated by SDS-PAGE. Wild-type GST-PI4KIIα-N-term purified a series of clients very similar to the S9/51A and L60/61A mutants (Figure 4A). However, GST-PI4KIIα-N-term-QD extracted a discrete cohort of proteins, suggesting that mock phosphorylation facilitated their binding (Figure 4A). The identity of these five proteins was established by liquid chromatography mass spectrometry. They were AGAP2 (a GTPase with GAP activity for ARF1/ARF5),[48–51] BRSK1 (a serine/threonine protein kinase),[52,53] CAMKV (an SV-localized pseudokinase),[54,55] TRIM3 (an E3 ligase localized to endosomes and Golgi apparatus),[56,57] and STOP175 (a microtubule stabilizing protein).[58–60] Further details on these interaction clients with respect to their vesicle trafficking function are provided in Table S1. Western blotting confirmed the identity of these interaction partners and their binding preference for GST-PI4KIIα-N-term-QD (Figures 4B–4F). Importantly, binding of these proteins to either GST-PI4KIIα-N-term-S9/51A or GST-PI4KIIα-N-term-L60/61A was similar to wild-type GST-PI4KIIα-N-term (Figures 4B–4F).

We next determined the interaction site for the GST-PI4KIIα-N-term-QD-specific binding partners by performing sequential truncations of GST-PI4KIIα-N-term-QD that contained either one or both of the pairs of GSK3β phosphorylation sites (Figure 5A). Full-length GST-PI4KIIα-N-term-QD extracted all five interaction partners. The shortest truncation, which encompassed the first 24 amino acids of the N terminus and therefore only one of the two GSK3β sites (Ser-5/9), displayed negligible binding (Figures 5B and 5C). In contrast, the first 58 residues displayed similar binding to full-length GST-PI4KIIα-N-term-QD (Figures 5B and 5C). Thus, the interaction

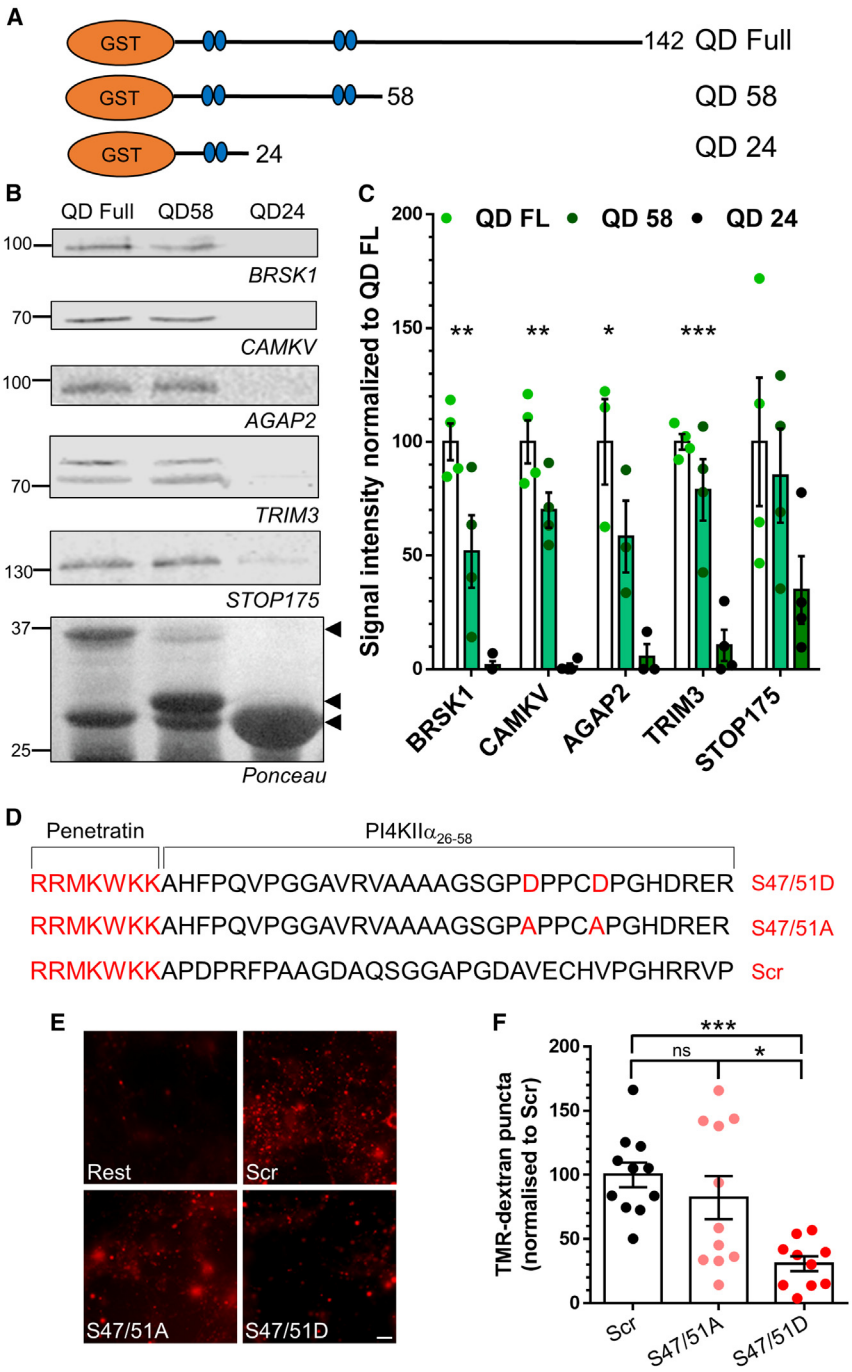

Figure 5. PI4KIIα controls ADBE via phospho-dependent interactions

(A–C) PI4KIIα GST-fusion proteins generated from either the full-length (FL) QD PI4KIIα N terminus or a truncated version (QD58, QD24) were incubated with nerve terminal lysates, and the presence of either BRSK1, CAMKV, AGAP2, TRIM3, or STOP175 was determined by western blotting. (B) Representative blots and Ponceau stain of GST fusion proteins (FL, QD58, and QD24 highlighted with arrows). (C) Quantification of binding ± SEM (all n = 4, except AGAP2 n = 3, ***p < 0.001, **p < 0.01, *p < 0.05, one-way ANOVA with Dunnett's multiple comparison test against FL).

(D–F) Primary cultures of CGNs were incubated with penetratin-tagged peptides corresponding to amino acids 26–58 of PI4KIIα with phosphomimic (S47/51D) or -null (S47/51A) substitutions or a Scr control peptide (D) for 30 min. CGNs were then stimulated with a train of 400 action potentials (40 Hz) in the presence of 50 μM TMR-dextran for 2 min. (E) Representative images of TMR-dextran loading, scale bar: 20 μm. (F) Mean TMR-dextran uptake as a proportion of total Scr uptake ± SEM (all n = 11, ***p < 0.001, *p < 0.05, one-way ANOVA with Dunnett's multiple comparison test against Scr).

site for these QD-specific interaction partners resides between residues 25 and 58 of the PI4KIIα N terminus, which contain both Ser-5/9 and Ser-47/51 sites.

To confirm that the PI4KIIα-dependent control of ADBE was via its protein interactions, we delivered peptides identical to the region of the N terminus that formed the binding platform for these phosphorylation-dependent clients. Three peptides were generated: a peptide with phosphomimetic substitutions (PI4KIIα$_{26-58}$-S47/51D), one with phospho-null substitutions (PI4KIIα$_{26-58}$-S47/51A), and a scrambled control (PI4KIIα$_{26-58}$-Scr). All peptides were delivered to CGNs using a penetratin sequence[14] (Figure 5D). PI4KIIα$_{26-58}$-S47/51A peptides had no effect on TMR-dextran uptake evoked by a 400 action potential stimulus (40 Hz) when compared with PI4KIIα$_{26-58}$-Scr (Figures 5E and 5F). In contrast, PI4KIIα$_{26-58}$-S47/51D produced a robust inhibition of TMR-dextran uptake (Figures 5E and 5F). The absence of inhibition by the PI4KIIα$_{26-58}$-S47/51A peptide was not due to an inability to enter CGNs since there was no difference in the efficiency of labeling between a fluorescein isothiocyanate (FITC)-tagged version of this peptide and PI4KIIα$_{26-58}$-S47/51D-FITC (Figure S4). Therefore the PI4KIIα$_{26-58}$-S47/51D peptide acts in a dominant-negative manner to disrupt protein-protein interactions with PI4KIIα, providing further evidence that PI4KIIα acts as a phospho-dependent adaptor hub for a series of presynaptic proteins to control ADBE.

Phosphorylation of Ser-47/51 on PI4KIIα controls ADBE

The inhibition of ADBE with the PI4KIIα$_{26-58}$-S47/51D peptide suggests that phosphorylation of Ser-47/51 is critical to control PI4KIIα protein-protein interactions and ADBE. Importantly, both Ser-47 and Ser-51 are physiologically relevant *in vivo* phosphorylation sites since both were identified in phosphoproteomic

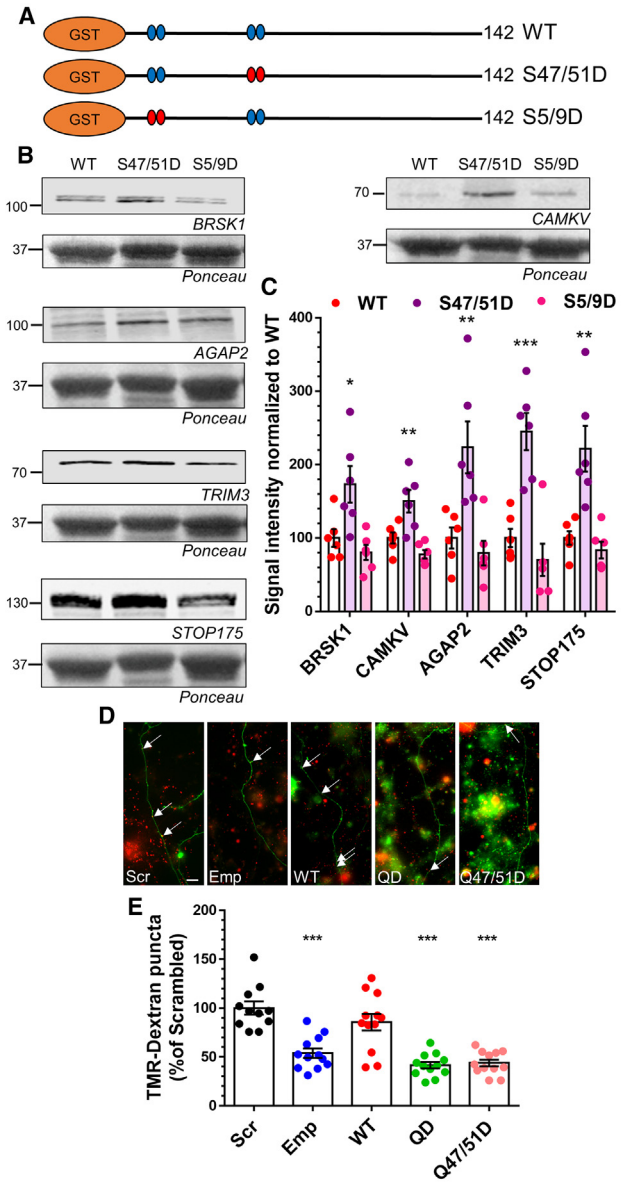

Figure 6. PI4KIIα controls ADBE via phosphorylation of Ser-47/51

(A–C) PI4KIIα GST-fusion proteins generated from either the FL PI4KIIα N terminus (WT) or versions with phosphomimic (S47/51D) or -null (S47/51A) substitutions were incubated with nerve terminal lysates, and the presence of either BRSK1, CAMKV, AGAP2, TRIM3, or STOP175 was determined by western blotting. (B) Representative blots with their respective GST fusion proteins (Ponceau). (C) Quantification of binding ± SEM (all n = 6, ***p < 0.001, **p < 0.01, *p < 0.05, one-way ANOVA with Dunnett's multiple comparison test against WT).

(D and E) Primary cultures of CGNs between 5 and 7 DIV were transfected with shRNA against either PI4KIIα or a Scr control. CGNs expressing PI4KIIα were co-transfected with either WT FLAG-PI4KIIα, PI4KIIα-QD, or PI4KIIα-S47/51D. At 8–10 DIV, CGNs were stimulated with a train of 400 action potentials (40 Hz) in the presence of 50 μM TMR-dextran for 2 min. (D) Representative images of TMR-dextran loading (red, arrows) in transfected neurons (green), scale bar: 20 μm. (E) Mean TMR-dextran uptake as a proportion of total Scr uptake ± SEM (all n = 12, except Scr n = 11, ***p < 0.001, one-way ANOVA with Dunnett's multiple comparison test against Scr).

screens of isolated nerve terminals.[61,62] To confirm their role, we performed affinity purifications from nerve terminal lysates using full-length GST-PI4KIIα-N-term with phosphomimetic substitutions at these sites (S47/51D; Figure 6A). All partners displayed enhanced binding to this mutant when compared with wild-type (Figures 6B and 6C). In contrast, a phosphomimetic mutant for sites Ser-5/9 (GST-PI4KIIα-N-term-S5/9D) bound the proteins at a similar level to wild type (Figures 6B and 6C). Therefore, the phosphorylation of residues Ser-47/51 create an interaction platform for five separate presynaptic molecules to bind PI4KIIα.

We next determined whether the Ser-47/51 sites were sufficient for PI4KIIα-dependent control of ADBE by expressing phosphomimetic mutants in PI4KIIα-depleted CGNs (Figure 6D). Depletion of endogenous PI4KIIα inhibited TMR-dextran uptake as observed previously (Figure 6E). Similarly, expression of exogenous wild-type PI4KIIα fully restored uptake, whereas PI4KIIα-QD did not (Figure 6E). Importantly, expression of PI4KIIα-S47/51D failed to restore TMR-dextran uptake (Figure 6E), indicating that these sites are key for the phosphorylation-dependent control of ADBE.

AGAP2 and CAMKV are required for ADBE

Thus far, we have demonstrated that mock phosphorylation of PI4KIIα at sites Ser-47/51 recruits a series of interaction partners and is unable to restore ADBE in PI4KIIα-depleted neurons. Therefore it is possible that these clients are recruited at rest via constitutive GSK3β phosphorylation, to be liberated by dephosphorylation of these sites to modulate ADBE during neuronal activity. In support, phosphoproteomic studies revealed that both Ser-47 and Ser-51 were dephosphorylated when isolated nerve terminals were depolarized.[61,62]

Therefore, we determined whether these phosphoregulated interaction partners were individually required for ADBE. This was achieved by generating shRNAs against all five clients and monitoring the effect of their individual depletion on evoked TMR-dextran uptake in CGNs (Figure 7A). All shRNAs reduced expression of their targets when assessed in a heterologous expression system (Figure S5). When the effect of knockdown on ADBE was assessed (using TMR-dextran uptake during 400 action potential [40 Hz] stimulation), depletion of either BRSK1, TRIM3, or STOP175 has no significant effect on the number of nerve terminals undergoing ADBE when compared with neurons expressing a scrambled shRNA (Figure 7B). In contrast, depletion of either AGAP2 or CAMKV resulted in a significant reduction in evoked TMR-dextran uptake (Figure 7B), strongly suggesting an independent role of these two proteins in ADBE. Thus, PI4KIIα controls recruitment of AGAP2 and CAMKV via the phosphorylation status of Ser-47/51 to perform specific roles in ADBE.

DISCUSSION

PI4KIIα accounts for the majority of PI4K activity in the mammalian brain, is enriched at both synapses and Golgi, and is responsible for the PI4K activity located on SVs.[24–27] However, a direct demonstration of an essential role in SV recycling has, to date, been absent. We reveal an essential activity-dependent requirement for PI4KIIα in the control of a specific endocytosis mode, ADBE. The lipid kinase activity of PI4KIIα was not required for

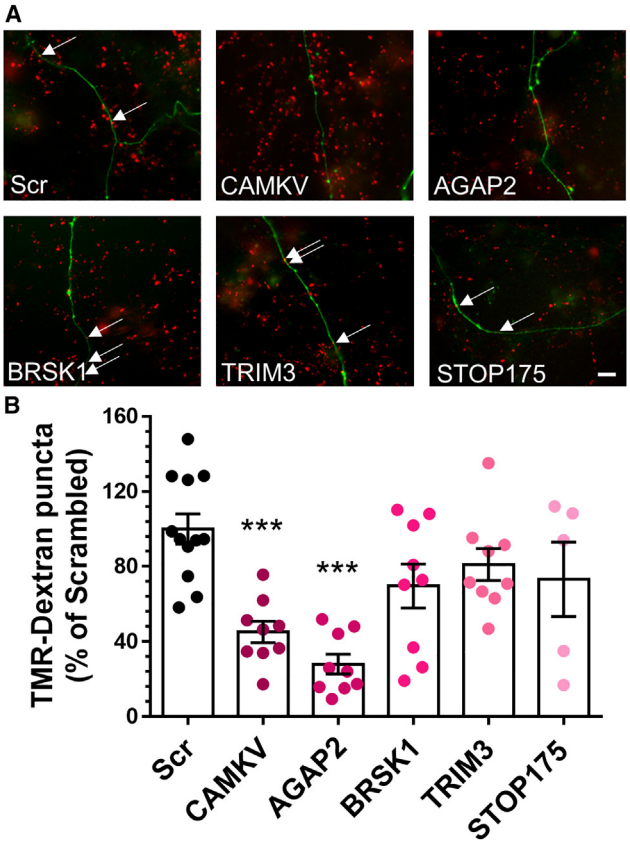

Figure 7. AGAP2 and CAMKV are essential for ADBE

Primary cultures of CGNs between 5 and 7 DIV were transfected with shRNA against either CAMKV, AGAP2, BRSK1, TRIM3, STOP175, or a Scr control. At 8–10 DIV, CGNs were stimulated with a train of 400 action potentials (40 Hz) in the presence of 50 μM TMR-dextran for 2 min.

(A) Representative images of TMR-dextran loading (red, arrows) in transfected neurons (green), scale bar: 20 μm.

(B) Mean TMR-dextran uptake as a proportion of total Scr uptake ± SEM (all n = 9, except STOP175 n = 5 and Scr n = 12, ***p < 0.001, **p < 0.01, one-way ANOVA with Dunnett's multiple comparison test against Scr).

this role, but instead, ADBE was controlled via the phosphorylation status of a GSK3β site on its N terminus (Ser-47/51). Phosphorylation of these residues triggers binding of five proteins, two of which (AGAP2, CAMKV) we discovered to be essential for ADBE in their own right. Therefore, PI4KIIα has the potential to act as a phospho-dependent protein interaction hub that silos key endocytosis molecules that are liberated during neuronal activity to drive ADBE.

A relatively surprising result was the rescue of ADBE by a kinase-dead mutant of PI4KIIα in our knockdown system. This result was corroborated with the absence of effect of a selective PI4KIIα inhibitor, PI-273, on TMR-dextran uptake. The lack of a role for lipid kinase activity contrasts with results from a PI4KII-null *Drosophila* model in which a kinase-dead mutant failed to restore KCl-evoked FM1-43 uptake.[63] However, evidence from non-neuronal cells suggest that while PI4KIIα knockdown does deplete PI(4)P, PI(4,5)P_2 levels can remain unaltered.[64] This may explain the rescue of ADBE observed with kinase-dead PI4KIIα mutants even though it has been proposed to require PI(4,5)P_2.[23]

In addition to an essential role in ADBE, PI4KIIα also appears to slow SV endocytosis since its depletion accelerates the retrieval of the genetically encoded reporter syp-pH only during high-frequency stimulation. A direct link to inhibited ADBE is unlikely since previous interventions that arrested this endocytosis mode did not impact the syp-pH response in CGNs, even during high-frequency stimulation.[44] Therefore, it is likely that PI4KIIα limits or slows the retrieval of SV cargo into SVs via modulation of either its phosphorylation status or its enzymatic activity. The former scenario is more likely, when one considers the requirement for PI(4,5)P_2 in SV cargo selection and clustering.[65] However, future work will be required to determine the underling mechanism for the repression of SV cargo retrieval.

Two phosphorylation-dependent PI4KIIα interactors were required for ADBE, AGAP2 and CAMKV. AGAP2 (also known as PIKE or centaurin-γ1A) is a modular protein that contains a GTPase, pleckstrin homology, and ArfGAP and Ankyrin repeat domains that is highly enriched in brain.[66] Neuron-specific functions include control of neurite outgrowth,[67] post-synaptic AMPA receptor trafficking,[68] and control of synaptic plasticity in animal models of fragile X syndrome.[69] A presynaptic role has been suggested in *Drosophila* where deletion of centaurin-γ results in increased evoked SV fusion and a reduction in presynaptic endosomes, potentially reflecting reduced ADBE.[70] Potential mechanisms for AGAP2 control of ADBE could be via a PH-domain-dependent control of AP-1 localization[48] (since AP-1 is required for ADBE[7,71]), via regulation of Akt[66] (a key negative regulator of ADBE[17]), or via a large number of presynaptic interaction partners, including GSK3.[72] Therefore, AGAP2 is perfectly positioned to control ADBE and associated endolysosomal trafficking of SV cargo via multiple complementary mechanisms.

CAMKV is an SV-associated calmodulin-binding pseudokinase[55] that is located at both the pre- and post-synapse.[55] Intriguingly, its expression is regulated by neuronal activity.[54] At the post-synapse, CAMKV is required for spine maintenance, with its binding to calmodulin essential for this role. CAMKV negatively regulates Rho kinase, with its activity inhibited by cdk5 phosphorylation.[54] Since cdk5 is a constitutively active kinase and an essential protein for ADBE,[11] this suggests that CAMKV activity may be regulated at the presynapse via its dephosphorylation by calcineurin. Therefore, it will be key for future investigations to determine the role of CAMKV phosphorylation in its control of both the presynaptic actin cytoskeleton and ADBE.

Depletion of three out of the five phospho-dependent PI4KIIα interacting proteins had no significant effect on TMR-dextran uptake, suggesting no direct role in ADBE. This was not due to inefficient knockdown since all shRNA sequences were previously validated[54,73–75] (except AGAP2) and depleted endogenous targets in cultured neuroblastoma cells (Figure S5). Indeed, depletion of STOP175 led to reductions in axon length and altered cell morphology, indicative of impaired function, in agreement with previous studies[59,60] (Figure S6). However, the absence of effect of knockdown of these phospho-dependent interactors suggests that they perform other roles linked to

PI4KIIα function at either the post-synapse or other stages of the endolysosomal pathway. In support, accurate post-synaptic trafficking of glutamatergic receptors requires PI4KIIα and is modulated by mutagenesis of these GSK3 sites.[34,76]

We predict that Ser-47 is phosphorylated in resting nerve terminals by constitutively active GSK3β after phosphorylation of Ser-51 by an undefined priming kinase.[34] Upon action potential invasion, these sites should be co-ordinately dephosphorylated by the calcium-dependent protein phosphatase calcineurin, in a similar manner to the GSK3β substrate dynamin-1.[16] This is supported in global phosphoproteomic screens from synaptosomes, which revealed that both Ser-47 and Ser-51 were dephosphorylated when nerve terminals were depolarized, whereas Ser-5 and Ser-9 were not.[61,62] Therefore, Ser-47 and Ser-51 are physiologically relevant *in vivo* phosphorylation sites that control both protein interactions and ADBE. Furthermore, PI4KIIα appears to be the latest member of the dephosphin group of presynaptic proteins[15] and suggests that GSK3β is a master regulator of ADBE, priming multiple molecules for synchronous activation during high-frequency neurotransmission.

For PI4KIIα to be regulated by neuronal activity, it must be present in a subcellular location. As stated above, PI4KIIα is located on both SVs and endosomes, suggesting that it will encounter activity-dependent calcium increases and activated calcineurin. Importantly, the membrane association of PI4KIIα is dependent on its palmitoylation,[77] with cholesterol being essential for this event.[78] SVs have an extremely high cholesterol content,[25] which will facilitate the enrichment of PI4KIIα on these organelles. Therefore, SV-localized PI4KIIα should be in a privileged location to be dephosphorylated by calcineurin during intense neuronal activity, liberating both AGAP2 and CAMKV to perform essential roles in ADBE. Thus, PI4KIIα is a phosphorylation-dependent interaction hub in ADBE that stockpiles an arsenal of key molecules in the correct location to perform their role.

Limitations of the study

One limitation of this study was our inability to demonstrate calcineurin-dependent dephosphorylation of Ser-47 during neuronal activity. A series of phospho-specific antibodies were generated against this site; however, extensive trials revealed that these did not accurately report phosphorylation of this residue. These included affinity purification, incubation with a non-phosphorylated form of the immunogenic peptide sequence, and coupling to immunogens to both N and C termini. Unfortunately, in all cases, these antibodies did not accurately report phosphorylation (confirmed by treating lysates with λ phosphatase). However, as stated above, two independent and unbiased phosphoproteomic screens revealed a significant activity-dependent decrease in the phosphorylation status of Ser-47 in isolated nerve terminals. A further limitation was that the impact of PI4KIIα knockdown on both Pr and presynaptic performance (measured using syp-pH) was not corroborated by monitoring the post-synaptic response to released glutamate via electrophysiology. The only viable way to determine this in primary neuronal culture would have been to transduce with PI4KIIα shRNA lentivirus and perform paired patch clamp recordings. However, the low efficiency of locating synaptic partners using this approach precluded this approach. Other alternatives were considered, such as delivery of lentivirus to mouse brain via stereotaxic surgery and preparing acute slices from the transduced circuits. However, since syp-pH had already provided a direct readout of SV fusion and rundown of presynaptic performance in PI4KIIα-depleted neurons, we opted not to perform this additional analysis.

STAR★METHODS

Detailed methods are provided in the online version of this paper and include the following:

- KEY RESOURCES TABLE
- RESOURCE AVAILABILITY
  - Lead contact
  - Materials availability
  - Data and code availability
- EXPERIMENTAL MODEL AND STUDY PARTICIPANT DETAILS
  - Animals
  - Primary tissue culture
  - Synaptosome preparation
  - Cell lines
- METHOD DETAILS
  - Materials
  - Transfection and viral transduction
  - Lentiviral particle production and transduction
  - Single cell TMR-dextran imaging
  - TMR-dextran field imaging
  - Morphological analysis of CGN nerve terminals
  - Syp-pH imaging
  - Quantification of knockdown of PI4KIIα interaction partners
  - Immunofluorescence
  - GST-fusion protein expression and affinity purification of nerve terminal proteins
  - Western blotting
  - In-gel digestion and LC MS identification of proteins
- QUANTIFICATION AND STATISTICAL ANALYSIS

SUPPLEMENTAL INFORMATION

Supplemental information can be found online at https://doi.org/10.1016/j.celrep.2023.112633.

ACKNOWLEDGMENTS

This research was funded by the Wellcome Trust (Investigator Award to M.A.C., 204954/Z/16/Z) and Epilepsy Research UK (P2003). For the purpose of open access, the author has applied a CC-BY public copyright license to any author-accepted manuscript version arising from this submission. J.C.N.-F. was supported by a studentship from the Biotechnology and Biological Sciences Research Council.

AUTHOR CONTRIBUTIONS

Conceptualization, M.A.C.; methodology, E.-M.B., J.C.N.-F., A.C., E.C.D., D.K., K.J.S., and M.A.C.; formal analysis, E.-M.B., J.C.N.-F., D.K., M.P., K.J.S., and M.A.C.; investigation, E.-M.B., J.C.N.-F., D.K., E.C.D., M.P., K.J.S., and M.A.C.; resources, M.A.C. and A.C.; writing – original draft,

E.-M.B. and M.A.C.; writing – review & editing, all authors; funding acquisition, M.A.C.

DECLARATION OF INTERESTS

The authors declare no competing interests.

Received: March 31, 2022
Revised: April 4, 2023
Accepted: May 25, 2023
Published: June 13, 2023

REFERENCES

1. Chanaday, N.L., Cousin, M.A., Milosevic, I., Watanabe, S., and Morgan, J.R. (2019). The synaptic vesicle cycle revisited: new insights into the modes and mechanisms. J. Neurosci. *39*, 8209–8216. https://doi.org/10.1523/jneurosci.1158-19.2019.
2. Kononenko, N.L., and Haucke, V. (2015). Molecular mechanisms of presynaptic membrane retrieval and synaptic vesicle reformation. Neuron *85*, 484–496. https://doi.org/10.1016/j.neuron.2014.12.016.
3. Watanabe, S., Rost, B.R., Camacho-Pérez, M., Davis, M.W., Söhl-Kielczynski, B., Rosenmund, C., and Jorgensen, E.M. (2013). Ultrafast endocytosis at mouse hippocampal synapses. Nature *504*, 242–247. https://doi.org/10.1038/nature12809.
4. Soykan, T., Kaempf, N., Sakaba, T., Vollweiter, D., Goerdeler, F., Puchkov, D., Kononenko, N.L., and Haucke, V. (2017). Synaptic vesicle endocytosis occurs on multiple timescales and is mediated by formin-dependent actin assembly. Neuron *93*, 854–866.e4. https://doi.org/10.1016/j.neuron.2017.02.011.
5. Clayton, E.L., Evans, G.J.O., and Cousin, M.A. (2008). Bulk synaptic vesicle endocytosis is rapidly triggered during strong stimulation. J. Neurosci. *28*, 6627–6632. https://doi.org/10.1523/jneurosci.1445-08.2008.
6. Watanabe, S., Trimbuch, T., Camacho-Pérez, M., Rost, B.R., Brokowski, B., Söhl-Kielczynski, B., Felies, A., Davis, M.W., Rosenmund, C., and Jorgensen, E.M. (2014). Clathrin regenerates synaptic vesicles from endosomes. Nature *515*, 228–233. https://doi.org/10.1038/nature13846.
7. Ivanova, D., Dobson, K.L., Gajbhiye, A., Davenport, E.C., Hacker, D., Ultanir, S.K., Trost, M., and Cousin, M.A. (2021). Control of synaptic vesicle release probability via VAMP4 targeting to endolysosomes. Sci. Adv. *7*, eabf3873. https://doi.org/10.1126/sciadv.abf3873.
8. Clayton, E.L., and Cousin, M.A. (2009). Quantitative monitoring of activity-dependent bulk endocytosis of synaptic vesicle membrane by fluorescent dextran imaging. J. Neurosci. Methods *185*, 76–81. https://doi.org/10.1016/j.jneumeth.2009.09.016.
9. Kokotos, A.C., and Cousin, M.A. (2015). Synaptic vesicle generation from central nerve terminal endosomes. Traffic *16*, 229–240. https://doi.org/10.1111/tra.12235.
10. Xue, J., Graham, M.E., Novelle, A.E., Sue, N., Gray, N., McNiven, M.A., Smillie, K.J., Cousin, M.A., and Robinson, P.J. (2011). Calcineurin selectively docks with the dynamin Ixb splice variant to regulate activity-dependent bulk endocytosis. J. Biol. Chem. *286*, 30295–30303. https://doi.org/10.1074/jbc.M111.273110.
11. Evans, G.J.O., and Cousin, M.A. (2007). Activity-dependent control of slow synaptic vesicle endocytosis by cyclin-dependent kinase 5. J. Neurosci. *27*, 401–411. https://doi.org/10.1523/jneurosci.3809-06.2007.
12. Wu, X.S., Zhang, Z., Zhao, W.D., Wang, D., Luo, F., and Wu, L.G. (2014). Calcineurin is universally involved in vesicle endocytosis at neuronal and nonneuronal secretory cells. Cell Rep. *7*, 982–988. https://doi.org/10.1016/j.celrep.2014.04.020.
13. Sun, T., Wu, X.S., Xu, J., McNeil, B.D., Pang, Z.P., Yang, W., Bai, L., Qadri, S., Molkentin, J.D., Yue, D.T., and Wu, L.G. (2010). The role of calcium/calmodulin-activated calcineurin in rapid and slow endocytosis at central synapses. J. Neurosci. *30*, 11838–11847. https://doi.org/10.1523/JNEUROSCI.1481-10.2010.
14. Clayton, E.L., Anggono, V., Smillie, K.J., Chau, N., Robinson, P.J., and Cousin, M.A. (2009). The phospho-dependent dynamin-syndapin interaction triggers activity-dependent bulk endocytosis of synaptic vesicles. J. Neurosci. *29*, 7706–7717. https://doi.org/10.1523/jneurosci.1976-09.2009.
15. Cousin, M.A., and Robinson, P.J. (2001). The dephosphins: dephosphorylation by calcineurin triggers synaptic vesicle endocytosis. Trends Neurosci. *24*, 659–665. https://doi.org/10.1016/s0166-2236(00)01930-5.
16. Clayton, E.L., Sue, N., Smillie, K.J., O'Leary, T., Bache, N., Cheung, G., Cole, A.R., Wyllie, D.J., Sutherland, C., Robinson, P.J., and Cousin, M.A. (2010). Dynamin I phosphorylation by GSK3 controls activity-dependent bulk endocytosis of synaptic vesicles. Nat. Neurosci. *13*, 845–851. https://doi.org/10.1038/nn.2571.
17. Smillie, K.J., and Cousin, M.A. (2012). Akt/PKB controls the activity-dependent bulk endocytosis of synaptic vesicles. Traffic *13*, 1004–1011. https://doi.org/10.1111/j.1600-0854.2012.01365.x.
18. Smillie, K.J., Pawson, J., Perkins, E.M., Jackson, M., and Cousin, M.A. (2013). Control of synaptic vesicle endocytosis by an extracellular signalling molecule. Nat. Commun. *4*, 2394. https://doi.org/10.1038/ncomms3394.
19. Lauwers, E., Goodchild, R., and Verstreken, P. (2016). Membrane lipids in presynaptic function and disease. Neuron *90*, 11–25. https://doi.org/10.1016/j.neuron.2016.02.033.
20. Milosevic, I., Sørensen, J.B., Lang, T., Krauss, M., Nagy, G., Haucke, V., Jahn, R., and Neher, E. (2005). Plasmalemmal phosphatidylinositol-4,5-bisphosphate level regulates the releasable vesicle pool size in chromaffin cells. J. Neurosci. *25*, 2557–2565. https://doi.org/10.1523/jneurosci.3761-04.2005.
21. Walter, A.M., Müller, R., Tawfik, B., Wierda, K.D., Pinheiro, P.S., Nadler, A., McCarthy, A.W., Ziomkiewicz, I., Kruse, M., Reither, G., et al. (2017). Phosphatidylinositol 4,5-bisphosphate optical uncaging potentiates exocytosis. Elife *6*, e30203. https://doi.org/10.7554/eLife.30203.
22. Di Paolo, G., Moskowitz, H.S., Gipson, K., Wenk, M.R., Voronov, S., Obayashi, M., Flavell, R., Fitzsimonds, R.M., Ryan, T.A., and De Camilli, P. (2004). Impaired PtdIns(4,5)P2 synthesis in nerve terminals produces defects in synaptic vesicle trafficking. Nature *431*, 415–422. https://doi.org/10.1038/nature02896.
23. Gormal, R.S., Nguyen, T.H., Martin, S., Papadopulos, A., and Meunier, F.A. (2015). An acto-myosin II constricting ring initiates the fission of activity-dependent bulk endosomes in neurosecretory cells. J. Neurosci. *35*, 1380–1389. https://doi.org/10.1523/jneurosci.3228-14.2015.
24. Guo, J., Wenk, M.R., Pellegrini, L., Onofri, F., Benfenati, F., and De Camilli, P. (2003). Phosphatidylinositol 4-kinase type IIalpha is responsible for the phosphatidylinositol 4-kinase activity associated with synaptic vesicles. Proc. Natl. Acad. Sci. USA *100*, 3995–4000. https://doi.org/10.1073/pnas.0230488100.
25. Takamori, S., Holt, M., Stenius, K., Lemke, E.A., Grønborg, M., Riedel, D., Urlaub, H., Schenck, S., Brügger, B., Ringler, P., et al. (2006). Molecular anatomy of a trafficking organelle. Cell *127*, 831–846. https://doi.org/10.1016/j.cell.2006.10.030.
26. Salazar, G., Craige, B., Wainer, B.H., Guo, J., De Camilli, P., and Faundez, V. (2005). Phosphatidylinositol-4-kinase type II alpha is a component of adaptor protein-3-derived vesicles. Mol. Biol. Cell *16*, 3692–3704. https://doi.org/10.1091/mbc.e05-01-0020.
27. Larimore, J., Tornieri, K., Ryder, P.V., Gokhale, A., Zlatic, S.A., Craige, B., Lee, J.D., Talbot, K., Pare, J.F., Smith, Y., and Faundez, V. (2011). The schizophrenia susceptibility factor dysbindin and its associated complex sort cargoes from cell bodies to the synapse. Mol. Biol. Cell *22*, 4854–4867. https://doi.org/10.1091/mbc.E11-07-0592.
28. Craige, B., Salazar, G., and Faundez, V. (2008). Phosphatidylinositol-4-kinase type II alpha contains an AP-3-sorting motif and a kinase domain that

are both required for endosome traffic. Mol. Biol. Cell *19*, 1415–1426. https://doi.org/10.1091/mbc.e07-12-1239.

29. Salazar, G., Zlatic, S., Craige, B., Peden, A.A., Pohl, J., and Faundez, V. (2009). Hermansky-Pudlak syndrome protein complexes associate with phosphatidylinositol 4-kinase type II alpha in neuronal and non-neuronal cells. J. Biol. Chem. *284*, 1790–1802. https://doi.org/10.1074/jbc.M805991200.
30. Newell-Litwa, K., Seong, E., Burmeister, M., and Faundez, V. (2007). Neuronal and non-neuronal functions of the AP-3 sorting machinery. J. Cell Sci. *120*, 531–541. https://doi.org/10.1242/jcs.03365.
31. Minogue, S. (2018). The many roles of type II phosphatidylinositol 4-kinases in membrane trafficking: new tricks for old dogs. Bioessays *40*, 1700145. https://doi.org/10.1002/bies.201700145.
32. Ryder, P.V., Vistein, R., Gokhale, A., Seaman, M.N., Puthenveedu, M.A., and Faundez, V. (2013). The WASH complex, an endosomal Arp2/3 activator, interacts with the Hermansky-Pudlak syndrome complex BLOC-1 and its cargo phosphatidylinositol-4-kinase type IIalpha. Mol. Biol. Cell *24*, 2269–2284. https://doi.org/10.1091/mbc.E13-02-0088.
33. Mössinger, J., Wieffer, M., Krause, E., Freund, C., Gerth, F., Krauss, M., and Haucke, V. (2012). Phosphatidylinositol 4-kinase IIα function at endosomes is regulated by the ubiquitin ligase Itch. EMBO Rep. *13*, 1087–1094. https://doi.org/10.1038/embor.2012.164.
34. Robinson, J.W., Leshchyns'ka, I., Farghaian, H., Hughes, W.E., Sytnyk, V., Neely, G.G., and Cole, A.R. (2014). PI4KIIalpha phosphorylation by GSK3 directs vesicular trafficking to lysosomes. Biochem. J. *464*, 145–156. https://doi.org/10.1042/BJ20140497.
35. Granseth, B., Odermatt, B., Royle, S.J., and Lagnado, L. (2006). Clathrin-mediated endocytosis is the dominant mechanism of vesicle retrieval at hippocampal synapses. Neuron *51*, 773–786. https://doi.org/10.1016/j.neuron.2006.08.029.
36. Atluri, P.P., and Ryan, T.A. (2006). The kinetics of synaptic vesicle reacidification at hippocampal nerve terminals. J. Neurosci. *26*, 2313–2320. https://doi.org/10.1523/JNEUROSCI.4425-05.2006.
37. Egashira, Y., Takase, M., and Takamori, S. (2015). Monitoring of vacuolar-type H+ ATPase-mediated proton influx into synaptic vesicles. J. Neurosci. *35*, 3701–3710. https://doi.org/10.1523/JNEUROSCI.4160-14.2015.
38. McAdam, R.L., Morton, A., Gordon, S.L., Alterman, J.F., Khvorova, A., Cousin, M.A., and Smillie, K.J. (2020). Loss of huntingtin function slows synaptic vesicle endocytosis in striatal neurons from the htt(Q140/Q140) mouse model of Huntington's disease. Neurobiol. Dis. *134*, 104637. https://doi.org/10.1016/j.nbd.2019.104637.
39. Zhao, H., Kim, Y., Park, J., Park, D., Lee, S.E., Chang, I., and Chang, S. (2014). SCAMP5 plays a critical role in synaptic vesicle endocytosis during high neuronal activity. J. Neurosci. *34*, 10085–10095. https://doi.org/10.1523/JNEUROSCI.2156-14.2014.
40. Imig, C., López-Murcia, F.J., Maus, L., García-Plaza, I.H., Mortensen, L.S., Schwark, M., Schwarze, V., Angibaud, J., Nägerl, U.V., Taschenberger, H., et al. (2020). Ultrastructural imaging of activity-dependent synaptic membrane-trafficking events in cultured brain slices. Neuron *108*, 843–860.e8. https://doi.org/10.1016/j.neuron.2020.09.004.
41. Körber, C., Horstmann, H., Sätzler, K., and Kuner, T. (2012). Endocytic structures and synaptic vesicle recycling at a central synapse in awake rats. Traffic *13*, 1601–1611. https://doi.org/10.1111/tra.12007.
42. Sankaranarayanan, S., and Ryan, T.A. (2001). Calcium accelerates endocytosis of vSNAREs at hippocampal synapses. Nat. Neurosci. *4*, 129–136. https://doi.org/10.1038/83949.
43. Hua, Y., Woehler, A., Kahms, M., Haucke, V., Neher, E., and Klingauf, J. (2013). Blocking endocytosis enhances short-term synaptic depression under conditions of normal availability of vesicles. Neuron *80*, 343–349. https://doi.org/10.1016/j.neuron.2013.08.010.
44. Nicholson-Fish, J.C., Kokotos, A.C., Gillingwater, T.H., Smillie, K.J., and Cousin, M.A. (2015). VAMP4 is an essential cargo molecule for activity-dependent bulk endocytosis. Neuron *88*, 973–984. https://doi.org/10.1016/j.neuron.2015.10.043.
45. Bonnycastle, K., Kind, P.C., and Cousin, M.A. (2022). FMRP sustains presynaptic function via control of activity-dependent bulk endocytosis. J. Neurosci. *42*, 1618–1628. https://doi.org/10.1523/jneurosci.0852-21.2021.
46. Minogue, S., Waugh, M.G., De Matteis, M.A., Stephens, D.J., Berditchevski, F., and Hsuan, J.J. (2006). Phosphatidylinositol 4-kinase is required for endosomal trafficking and degradation of the EGF receptor. J. Cell Sci. *119*, 571–581. https://doi.org/10.1242/jcs.02752.
47. Li, J., Gao, Z., Zhao, D., Zhang, L., Qiao, X., Zhao, Y., Ding, H., Zhang, P., Lu, J., Liu, J., et al. (2017). PI-273, a substrate-competitive, specific small-molecule inhibitor of PI4KIIα, inhibits the growth of breast cancer cells. Cancer Res. *77*, 6253–6266. https://doi.org/10.1158/0008-5472.Can-17-0484.
48. Nie, Z., Fei, J., Premont, R.T., and Randazzo, P.A. (2005). The Arf GAPs AGAP1 and AGAP2 distinguish between the adaptor protein complexes AP-1 and AP-3. J. Cell Sci. *118*, 3555–3566. https://doi.org/10.1242/jcs.02486.
49. Nie, Z., and Randazzo, P.A. (2006). Arf GAPs and membrane traffic. J. Cell Sci. *119*, 1203–1211. https://doi.org/10.1242/jcs.02924.
50. Shiba, Y., Römer, W., Mardones, G.A., Burgos, P.V., Lamaze, C., and Johannes, L. (2010). AGAP2 regulates retrograde transport between early endosomes and the TGN. J. Cell Sci. *123*, 2381–2390. https://doi.org/10.1242/jcs.057778.
51. Wu, Y., Zhao, Y., Ma, X., Zhu, Y., Patel, J., and Nie, Z. (2013). The Arf GAP AGAP2 interacts with β-arrestin2 and regulates β2-adrenergic receptor recycling and ERK activation. Biochem. J. *452*, 411–421. https://doi.org/10.1042/bj20121004.
52. Inoue, E., Mochida, S., Takagi, H., Higa, S., Deguchi-Tawarada, M., Takao-Rikitsu, E., Inoue, M., Yao, I., Takeuchi, K., Kitajima, I., et al. (2006). SAD: a presynaptic kinase associated with synaptic vesicles and the active zone cytomatrix that regulates neurotransmitter release. Neuron *50*, 261–275. https://doi.org/10.1016/j.neuron.2006.03.018.
53. Mochida, S., Hida, Y., Tanifuji, S., Hagiwara, A., Hamada, S., Abe, M., Ma, H., Yasumura, M., Kitajima, I., Sakimura, K., and Ohtsuka, T. (2016). SAD-B phosphorylation of CAST controls active zone vesicle recycling for synaptic depression. Cell Rep. *16*, 2901–2913. https://doi.org/10.1016/j.celrep.2016.08.020.
54. Liang, Z., Zhan, Y., Shen, Y., Wong, C.C.L., Yates, J.R., 3rd, Plattner, F., Lai, K.O., and Ip, N.Y. (2016). The pseudokinase CaMKv is required for the activity-dependent maintenance of dendritic spines. Nat. Commun. *7*, 13282. https://doi.org/10.1038/ncomms13282.
55. Godbout, M., Erlander, M.G., Hasel, K.W., Danielson, P.E., Wong, K.K., Battenberg, E.L., Foye, P.E., Bloom, F.E., and Sutcliffe, J.G. (1994). 1G5: a calmodulin-binding, vesicle-associated, protein kinase-like protein enriched in forebrain neurites. J. Neurosci. *14*, 1–13. https://doi.org/10.1523/jneurosci.14-01-00001.1994.
56. Schreiber, J., Végh, M.J., Dawitz, J., Kroon, T., Loos, M., Labonté, D., Li, K.W., Van Nierop, P., Van Diepen, M.T., De Zeeuw, C.I., et al. (2015). Ubiquitin ligase TRIM3 controls hippocampal plasticity and learning by regulating synaptic γ-actin levels. J. Cell Biol. *211*, 569–586. https://doi.org/10.1083/jcb.201506048.
57. Labonté, D., Thies, E., Pechmann, Y., Groffen, A.J., Verhage, M., Smit, A.B., van Kesteren, R.E., and Kneussel, M. (2013). TRIM3 regulates the motility of the kinesin motor protein KIF21B. PLoS One *8*, e75603. https://doi.org/10.1371/journal.pone.0075603.
58. Guillaud, L., Bosc, C., Fourest-Lieuvin, A., Denarier, E., Pirollet, F., Lafanechère, L., and Job, D. (1998). STOP proteins are responsible for the high degree of microtubule stabilization observed in neuronal cells. J. Cell Biol. *142*, 167–179. https://doi.org/10.1083/jcb.142.1.167.
59. Deloulme, J.C., Gory-Fauré, S., Mauconduit, F., Chauvet, S., Jonckheere, J., Boulan, B., Mire, E., Xue, J., Jany, M., Maucler, C., et al. (2015).

Microtubule-associated protein 6 mediates neuronal connectivity through Semaphorin 3E-dependent signalling for axonal growth. Nat. Commun. *6*, 7246. https://doi.org/10.1038/ncomms8246.

60. Tortosa, E., Adolfs, Y., Fukata, M., Pasterkamp, R.J., Kapitein, L.C., and Hoogenraad, C.C. (2017). Dynamic palmitoylation targets MAP6 to the axon to promote microtubule stabilization during neuronal polarization. Neuron *94*, 809–825.e7. https://doi.org/10.1016/j.neuron.2017.04.042.
61. Engholm-Keller, K., Waardenberg, A.J., Müller, J.A., Wark, J.R., Fernando, R.N., Arthur, J.W., Robinson, P.J., Dietrich, D., Schoch, S., and Graham, M.E. (2019). The temporal profile of activity-dependent presynaptic phospho-signalling reveals long-lasting patterns of poststimulus regulation. PLoS Biol. *17*, e3000170. https://doi.org/10.1371/journal.pbio.3000170.
62. Silbern, I., Pan, K.T., Fiosins, M., Bonn, S., Rizzoli, S.O., Fornasiero, E.F., Urlaub, H., and Jahn, R. (2021). Protein phosphorylation in depolarized synaptosomes: dissecting primary effects of calcium from synaptic vesicle cycling. Mol. Cell. Proteomics *20*, 100061. https://doi.org/10.1016/j.mcpro.2021.100061.
63. Cantarutti, K.C., Burgess, J., Brill, J.A., and Dason, J.S. (2018). Type II phosphatidylinositol 4-kinase regulates nerve terminal growth and synaptic vesicle recycling. J. Neurogenet. *32*, 230–235. https://doi.org/10.1080/01677063.2018.1502762.
64. Ketel, K., Krauss, M., Nicot, A.S., Puchkov, D., Wieffer, M., Müller, R., Subramanian, D., Schultz, C., Laporte, J., and Haucke, V. (2016). A phosphoinositide conversion mechanism for exit from endosomes. Nature *529*, 408–412. https://doi.org/10.1038/nature16516.
65. Posor, Y., Eichhorn-Grünig, M., and Haucke, V. (2015). Phosphoinositides in endocytosis. Biochim. Biophys. Acta *1851*, 794–804. https://doi.org/10.1016/j.bbalip.2014.09.014.
66. Ahn, J.Y., and Ye, K. (2005). PIKE GTPase signaling and function. Int. J. Biol. Sci. *1*, 44–50. https://doi.org/10.7150/ijbs.1.44.
67. Dwane, S., Durack, E., O'Connor, R., and Kiely, P.A. (2014). RACK1 promotes neurite outgrowth by scaffolding AGAP2 to FAK. Cell. Signal. *26*, 9–18. https://doi.org/10.1016/j.cellsig.2013.08.036.
68. Chan, C.B., Chen, Y., Liu, X., Tang, X., Lee, C.W., Mei, L., and Ye, K. (2011). PIKE-mediated PI3-kinase activity is required for AMPA receptor surface expression. EMBO J. *30*, 4274–4286. https://doi.org/10.1038/emboj.2011.281.
69. Gross, C., Chang, C.W., Kelly, S.M., Bhattacharya, A., McBride, S.M.J., Danielson, S.W., Jiang, M.Q., Chan, C.B., Ye, K., Gibson, J.R., et al. (2015). Increased expression of the PI3K enhancer PIKE mediates deficits in synaptic plasticity and behavior in fragile X syndrome. Cell Rep. *11*, 727–736. https://doi.org/10.1016/j.celrep.2015.03.060.
70. Homma, M., Nagashima, S., Fukuda, T., Yanagi, S., Miyakawa, H., Suzuki, E., and Morimoto, T. (2014). Downregulation of Centaurin gamma1A increases synaptic transmission at Drosophila larval neuromuscular junctions. Eur. J. Neurosci. *40*, 3158–3170. https://doi.org/10.1111/ejn.12681.
71. Cheung, G., and Cousin, M.A. (2012). Adaptor protein complexes 1 and 3 are essential for generation of synaptic vesicles from activity-dependent bulk endosomes. J. Neurosci. *32*, 6014–6023. https://doi.org/10.1523/JNEUROSCI.6305-11.2012.
72. Wilkinson, B., Li, J., and Coba, M.P. (2017). Synaptic GAP and GEF complexes cluster proteins essential for GTP signaling. Sci. Rep. *7*, 5272. https://doi.org/10.1038/s41598-017-05588-3.
73. Schwenk, B.M., Lang, C.M., Hogl, S., Tahirovic, S., Orozco, D., Rentzsch, K., Lichtenthaler, S.F., Hoogenraad, C.C., Capell, A., Haass, C., and Edbauer, D. (2014). The FTLD risk factor TMEM106B and MAP6 control dendritic trafficking of lysosomes. EMBO J. *33*, 450–467. https://doi.org/10.1002/embj.201385857.
74. Choudhary, A., Hu He, K., Mertins, P., Udeshi, N.D., Dančík, V., Fomina-Yadlin, D., Kubicek, S., Clemons, P.A., Schreiber, S.L., Carr, S.A., and Wagner, B.K. (2014). Quantitative-proteomic comparison of alpha and Beta cells to uncover novel targets for lineage reprogramming. PLoS One *9*, e95194. https://doi.org/10.1371/journal.pone.0095194.
75. Hung, A.Y., Sung, C.C., Brito, I.L., and Sheng, M. (2010). Degradation of postsynaptic scaffold GKAP and regulation of dendritic spine morphology by the TRIM3 ubiquitin ligase in rat hippocampal neurons. PLoS One *5*, e9842. https://doi.org/10.1371/journal.pone.0009842.
76. Amici, M., Lee, Y., Pope, R.J.P., Bradley, C.A., Cole, A., and Collingridge, G.L. (2021). GSK-3beta regulates the synaptic expression of NMDA receptors via phosphorylation of phosphatidylinositol 4 kinase type IIalpha. Eur. J. Neurosci. *54*, 6815–6825. https://doi.org/10.1111/ejn.14841.
77. Barylko, B., Mao, Y.S., Wlodarski, P., Jung, G., Binns, D.D., Sun, H.Q., Yin, H.L., and Albanesi, J.P. (2009). Palmitoylation controls the catalytic activity and subcellular distribution of phosphatidylinositol 4-kinase II {alpha. J. Biol. Chem. *284*, 9994–10003. https://doi.org/10.1074/jbc.M900724200.
78. Lu, D., Sun, H.Q., Wang, H., Barylko, B., Fukata, Y., Fukata, M., Albanesi, J.P., and Yin, H.L. (2012). Phosphatidylinositol 4-kinase IIalpha is palmitoylated by Golgi-localized palmitoyltransferases in cholesterol-dependent manner. J. Biol. Chem. *287*, 21856–21865. https://doi.org/10.1074/jbc.M112.348094.
79. Ivanova, D., Imig, C., Camacho, M., Reinhold, A., Guhathakurta, D., Montenegro-Venegas, C., Cousin, M.A., Gundelfinger, E.D., Rosenmund, C., Cooper, B., and Fejtova, A. (2020). CtBP1-Mediated membrane fission contributes to effective recycling of synaptic vesicles. Cell Rep. *30*, 2444–2459.e7. https://doi.org/10.1016/j.celrep.2020.01.079.
80. Rappsilber, J., Mann, M., and Ishihama, Y. (2007). Protocol for micro-purification, enrichment, pre-fractionation and storage of peptides for proteomics using StageTips. Nat. Protoc. *2*, 1896–1906. https://doi.org/10.1038/nprot.2007.261.
81. Dwyer, B.J., Jarman, E.J., Gogoi-Tiwari, J., Ferreira-Gonzalez, S., Boulter, L., Guest, R.V., Kendall, T.J., Kurian, D., Kilpatrick, A.M., Robson, A.J., et al. (2021). TWEAK/Fn14 signalling promotes cholangiocarcinoma niche formation and progression. J. Hepatol. *74*, 860–872. https://doi.org/10.1016/j.jhep.2020.11.018.

STAR★METHODS

KEY RESOURCES TABLE

REAGENT or RESOURCE	SOURCE	IDENTIFIER
Antibodies		
Rabbit anti- PI4KIIα	Prof. Victor Faundez (Emory University, USA)	N/A
Rat anti- PI4KIIα	Prof. Shane Minogue (University College London, UK)	N/A
Rabbit anti-SV2A	Abcam, UK	Cat # ab32942 RRID: AB_778192
Mouse anti-actin	Sigma-Aldrich, UK	Cat # A3854 RRID:AB_262011
Rabbit anti-EGFP	Abcam, UK	Cat # ab290 RRID:AB_303395
Chicken anti-EGFP	Abcam, UK	Cat # ab13970 RRID:AB_300798
Rabbit anti-AGAP2	Novus Biologicals, UK	Cat # NBP2-24498
Mouse anti-STOP175	Cell Signaling Technology, UK	Cat # 4265 RRID:AB_2140993
Rabbit anti-CAMKV	Abcam, UK	Cat # ab69564 RRID:AB_1267918
Rabbit anti-BRSK1	Abcam, UK	Cat # ab206298
Rabbit anti-TRIM3	Abcam, UK	Cat # ab111840 RRID:AB_10860004
Mouse anti-synaptotagmin-1	Abcam, UK	Cat # ab13259 RRID:AB_299799
Rabbit anti-synaptotagmin-1	Synaptic Systems, Germany	Cat # 105103 RRID:AB_11042457
Anti FLAG	Sigma-Aldrich, UK	Cat #F1804 RRID:AB_262044
Donkey anti-rabbit IgG IR Dye 800 CW	LI-COR, UK	Cat # 925–32213, RRID:AB_2715510
Donkey anti-goat IgG IR Dye 800 CW	LI-COR, UK	Cat # 925–32214, RRID:AB_2687553
Donkey anti-mouse IgG IR Dye 800 CW	LI-COR, UK	Cat # 925–32212, RRID:AB_2716622
Donkey anti-mouse IgG IR Dye 680RD	LI-COR, UK	Cat # 925–68072, RRID:AB_2814912
Donkey anti-mouse Alexa Fluor 647	Thermo Fisher Scientific, UK	Cat # A-32787 RRID:AB_2762830
Goat anti-rabbit Alexa Fluor 488	Thermo Fisher Scientific, UK	Cat # A-11008 RRID:AB_143165
Goat anti-chicken Alexa Fluor 488	Thermo Fisher Scientific, UK	Cat# A-11039, RRID:AB_142924
Chemicals, Peptides, and Recombinant Proteins		
Bafilomycin A1	Cayman Chemical Company, USA	Cat # 11038
Boric Acid	Sigma Aldrich, UK	Cat #B6768
Bovine serum albumin	Roche Diagnostics GmbH, Germany	Cat # 10735078001
β-mercaptoethanol	Sigma Aldrich, UK	Cat #M3250
Bromophenol blue	Sigma Aldrich, UK	Cat #B0126
Cytosine arabinofuranoside (AraC)	Sigma Aldrich, UK	Cat #C1768
D-(+)-Glucose	Sigma Aldrich, UK	Cat #G5767
DNAse	Sigma Aldrich, UK	Cat #D5025
Dimethyl sulfoxide	Sigma Aldrich, UK	Cat #D8418
Durcupan resin	Sigma Aldrich, Gillingham, UK	Cat# 44610
EDTA	Sigma Aldrich, UK	Cat #E5134
EGTA	Sigma Aldrich, UK	Cat #E4378

(*Continued on next page*)

Continued

REAGENT or RESOURCE	SOURCE	IDENTIFIER
DMEM	Thermo-Fischer Scientific, UK	Cat # 41966
FluorSave Reagent	Millipore, Darmstadt, Germany	Cat # 345789
Fetal Bovine serum (FBS)	BioSera, France	Cat #S1810-500
Glutaraldehyde	Agar Scientific, Stanstead, UK	Cat# AGR1020
GSH-Sepharose beads	GE-Healthcare, UK	Cat # GE-170756-01
HEPES	Fisher Bioreagents, UK	Cat # BP3101
L-glutamine	Gibco, UK	Cat # 25030-024
Lipofectamine 2000	ThermoFisher Scientific, UK	Cat # 11668027
Leupeptin	Sigma Aldrich, UK	Cat #L2884
MEM, no glutamine	Gibco, UK	Cat # 11090081
NaCl	Sigma Aldrich, UK	Cat #S7636
Na_2HPO_4	Acros Organic, UK	Cat # 448140010
NaH_2PO_4	Acros Organic, UK	Cat # 447760010
Nitrocellulose membrane	Amersham Biosciences, UK	Cat # 10600002,
Odyssey Intercept-PBS buffer	Licor Biosciences, USA	Cat # 927-70001
Opti-MEM	Thermo-Fischer Scientific, UK	Cat # 11524456
Osmium tetroxide	TAAB laboratory and microscopy, Aldermaston, UK	Cat# O015/1
Paraformaldehyde	Electron Microscopy Sciences, USA	Cat # 15710
Penicillin/streptomycin	Gibco, UK	Cat # 15140-122
Poly-D-lysine	Sigma Aldrich, UK	Cat #P7886
Polypropylene oxide	Electron Microscopy Sciences, Hatfield, USA	Cat# 20411
Ponceau S	Sigma Aldrich, UK	Cat #P7170
Phenylmethylsulfonyl fluoride	Thermo-Fischer Scientific, UK	Cat # 36978
Protease inhibitor mix	Sigma Aldrich, UK	Cat #P8849
PI-273	MedChemExpress, UK	Cat # HY103481
N-Tris-HCl (hydroxymethyl)-methyl-2-aminoethane sulfonic acid (TES)	Sigma Aldrich, UK	Cat #T1375
Tetramethylrhodamine (TMR) dextran, 40,000 MW	Life Technologies, UK	Cat #D1842
Tween 20	Sigma Aldrich, UK	Cat #P1375
Triton X-100	Sigma Aldrich, UK	Cat #T8787
Trypsin	Sigma Aldrich, UK	Cat #T9201
PI4KII$\alpha_{26\text{-}58}$ Scr	This paper	N/A
PI4KII$\alpha_{26\text{-}58}$ S47/51A	This paper	N/A
PI4KII$\alpha_{26\text{-}58}$ S47/51D	This paper	N/A
PI4KII$\alpha_{26\text{-}58}$ S47/51A-FITC	This paper	N/A
PI4KII$\alpha_{26\text{-}58}$ S47/51D-FITC	This paper	N/A
Experimental models: organisms/strains		
Sprague-Dawley Rat	Charles River, UK	N/A
Recombinant DNA		
Syp-pH	Prof. Leon Lagnado (University of Sussex[35])	RRID:Addgene_24478
pSUPER mCerulean	Clayton et al.[16]	N/A
pSuper mCer Scrambled shRNA	Nicholson-Fish et al.[44]	N/A
pSuper mCer-shRNA AGAP2	This paper	N/A
pSuper mCer-shRNA CAMKV	Liang et al.[54]	N/A

(*Continued on next page*)

Continued

REAGENT or RESOURCE	SOURCE	IDENTIFIER
pSuper mCer-shRNA STOP175	Schwenk et al.[73]	N/A
pSuper mCer-shRNA BRSK1	Choudhary et al.[74]	N/A
pSuper mCer-shRNA TRIM3	Hung et al.[75]	N/A
pSuper shRNA PI4KIIα	Robinson et al.[34]	N/A
pRKV_PI4KIIα	Robinson et al.[34]	N/A
pLV[shRNA]-mCerulean-U6>PI4KIIa[shRNA]	This paper	N/A
pLV[shRNA]-mCerulean-U6>Scr[shRNA]	This paper	N/A
pRKV_PI4KIIα K152A	This paper	N/A
pRKV_PI4KIIα L60/61A	Robinson et al.[34]	N/A
pRKV_PI4KIIα S9/51A	Robinson et al.[34]	N/A
pRKV_PI4KIIα S5/9/47/51D (QD)	This paper	N/A
pRKV_PI4KIIα S47/51D	This paper	N/A
pGEX-KG	Dr. Colin Rickman (Heriot-Watt University, UK)	N/A
pGEX-KG PI4KIIα N terminus (amino acids 1–142)	This paper	N/A
pGEX-KG PI4KIIα N terminus (amino acids 1–24)	This paper	N/A
pGEX-KG PI4KIIα N terminus (amino acids 1–58)	This paper	N/A
pGEX-KG PI4KIIα N terminus S9/51A	This paper	N/A
pGEX-KG PI4KIIα N terminus L60/61A	This paper	N/A
pGEX-KG PI4KIIα N terminus QD	This paper	N/A
pGEX-KG PI4KIIα N terminus S5/9D	This paper	N/A
pGEX-KG PI4KIIα N terminus S47/51D	This paper	N/A
Software and algorithms		
Fiji	http://fiji.sc	RRID:SCR_002285
GraphPad Prism 8	https://www.graphpad.com	RRID:SCR_002798

RESOURCE AVAILABILITY

Lead contact

Further information and requests for resources and reagents should be directed to and will be fulfilled by the Lead Contact, Michael Cousin (m.cousin@ed.ac.uk).

Materials availability

All unique/stable reagents generated in this study are available from the lead contact without restriction.

Data and code availability

All data reported in this paper will be shared by the lead contact on request. This study does not report original code. Any additional information required to reanalyze the data reported in this paper will be provided by the lead contact upon request.

EXPERIMENTAL MODEL AND STUDY PARTICIPANT DETAILS

Animals

Wild-type Sprague-Dawley rats were obtained from an in-house colony at The University of Edinburgh. All animal work was performed in accordance with the UK Animal (Scientific Procedures) Act 1986, under Project Licence authority (PPL - 7008878) and was approved by the Animal Welfare and Ethical Review Body at the University of Edinburgh. All animals were killed by schedule 1 procedures; adults were killed by cervical dislocation followed by decapitation, whereas neonatal rat pups were killed by anesthetic overdose, with death confirmed via the destruction of the brain. Sprague-Dawley rat breeding colonies were housed in standard open top caging on a 14-h light/dark cycle (light 07:00–21:00) and were maintained on RM3 chow.

Primary tissue culture

Primary cultures of CGNs were prepared from the cerebella of 7-day old Sprague-Dawley rat pups of both sexes as described previously.[5] The cells were plated on PDL-coated glass-coverslips (VWR, Germany, ECN631-1584) inserted into 6-well tissue culture plates using ≈560,000 cells/coverslip for biochemical and ≈260,000 cells/coverslip for imaging experiments. CGNs were maintained at 37°C, 5% CO_2 in MEM based culture medium supplemented with 100 U/mL penicillin, 100 μg/mL streptomycin, 33 mM glucose, 25 mM KCl, 2 mM Glutamine, 10% fetal bovine serum and 10 μM cytosine-β-D-arabinofuranoside.

Synaptosome preparation

Forebrain synaptosomes were prepared from adult (>2 months) Sprague-Dawley rats of either sex. Briefly, forebrains were homogenised in Tris-buffered sucrose (0.32 M sucrose, 1 mM EDTA, 5 mM Tris, pH 7.4) and centrifuged at 1075 *g* for 10 min to pellet the nuclear fraction (P1). Next, the supernatant (S1) was centrifuged at 20,200 *g* for 15 min to pellet synaptosomes (P2).

Cell lines

Neuro2A (N2A) cells between passage number 20–32 were grown in DMEM based culture medium (supplemented with 100 U/mL penicillin, 100 μg/mL streptomycin, 10% fetal bovine serum) in a 5% CO2-controlled atmosphere at 37°C until fully confluent. They were then seeded in 6-well plates to obtain 70-80% confluency one day after plating and maintained in a 5% CO2-controlled atmosphere at 37°C in a cell culture incubator. HEK293T cells were grown in an identical media to N2A cells in a 5% CO2-controlled atmosphere at 37°C until fully confluent.

METHOD DETAILS

Materials

A pSUPER vector expressing shRNA against mouse and rat PI4KIIα was generated as described.[34] FLAG-tagged wild-type mouse PI4KIIα and associated shRNA-resistant mutants were generated as described.[34] Wild-type PI4KIIα N terminus (amino acids 1–142) was cloned into a PGEX-KG vector using XhoI and HindIII enzymes and the primers (restriction sites underlined – Sense AGGTGTCCTCGAGATGGACGAGACGAGCCCGCTAGTGT; antisense CGCACCTAAGCTTCTTCCACTGGAGCCCTGGTAGATGC). These primers were also used for PI4KIIα mutants with the following exceptions – PI4KIIα QUAD-D, Sense AGGTGTCCTCGAGATG GACGAGACGGACCCGCTAGTGG; PI4KIIα AA, Sense AGGTGTCCTCGAGATGGACGAGACGAGCCCGCTAGTGG.

Truncations of the GST PI4KIIα N terminus were generated by introducing a stop codon using site-directed mutagenesis after amino acids Ser-24 (PI4KIIα N-term(1–24)) or Arg-58 (PI4KIIα N-term(1–58)). The GST PI4KIIα N terminus SS47/51DD mutant was generated by excising the sequence encoding amino acids 1–26 from wild-type GST PI4KIIα N terminus using the enzymes HindIII and RsrII and ligating into QUAD-D GST PI4KIIα N terminus. GST PI4KIIα N terminus SS5/9DD mutant was generated in an identical manner, with the exception that the QUAD-D sequence was excised into wild-type GST PI4KIIα N terminus.

Knockdown vectors to the following targets were generated using a pSUPER vector which expressed the fluorescent protein mCerulean.[16] All sequences were obtained from previously validated sequences with the exception of AGAP2 which was generated via rational design. Sequences are (5′ to 3′ in all cases) - AGAP2 - AGAGGGGCCTTGTAATTTA, CAMKV, from[54] - GCCAAGAA CGAGATTGGAA; STOP175 from[73] - GGTGCAGATCAGCGTGACA; BRSK1 from[74] - CCTTGGACAAAGAAGAACAAA; TRIM3 from[75]- TGGACAAGCAGTTTCTGGT. A random scrambled shRNA sequence in the same mCerulean-pSUPER vector was employed as a control.[44] Lentiviral shRNA knockdown vectors were generated by VectorBuilder Inc. (Chicago, USA). PI4KIIα and scrambled shRNA sequences were inserted into a pLV plasmid co-expressing mCer.

Peptides corresponding to amino acids 26–58 of mouse PI4KIIα plus a penetratin tag (underlined) were generated with either phospho-mimetic (PI4KII$\alpha_{26\text{-}58}$-S47/51D; RRMKWKKAHFPQVPGGAVRVAAAAGSGPDPPCDPGHDRER) or –null (PI4KII$\alpha_{26\text{-}58}$-S47/51A; RRMKWKKAHFPQVPGGAVRVAAAAGSGPAPPCAPGHDRER) substitutions were generated by BioServUK Ltd. (Sheffield, UK). FITC-tagged versions (C-terminal tag) of PI4KII$\alpha_{26\text{-}58}$-S47/51A and PI4KII$\alpha_{26\text{-}58}$-S47/51D were also generated. A scrambled control against the phospho-mimetic sequence was also generated (PI4KII$\alpha_{26\text{-}58}$-Scr; RRMKWKKAPDPRFPAAGDAQSGGAPGDAVECH VPGHRRVP).

Pan- PI4KIIα antibodies used for immunohistochemistry were gifts from both Prof. Shane Minogue (1:200, rat hybridoma supernatant, University College London, UK) and Prof. Victor Faundez (1:500, polyclonal rabbit, purified, Emory University, USA). The following primary antibodies were also used for western blotting; actin (1:30000, Sigma-Aldrich, A3854, RRID:AB_262011); EGFP (1:5000, Abcam, ab290, RRID:AB_303395); AGAP2 (1:1000, Novus Biologicals, NBP2-24498); STOP175 (WB 1:1000, Cell Signaling Technology, 4265, RRID:AB_2140993); CAMKV (1:2000, Abcam ab69564, RRID:AB_1267918); BRSK1 (1:2000, Abcam, ab206298); TRIM3 (1:800, Abcam ab111840, RRID:AB_10860004). The following primary antibodies were used for immunohistochemistry; SV2A (1:500, Abcam ab32942, RRID: AB_778192); synaptotagmin-1 (1:500, Abcam, ab13259, RRID:AB_299799); synaptotagmin-1 (1:200, Synaptic Systems, 105103); FLAG (1:500, Sigma-Aldrich, F1804, RRID:AB_262044); EGFP (1:2000, Abcam, ab13970, RRID:AB_300798). The following secondary antibodies were used for western blotting; donkey anti-rabbit IgG IR Dye 800 CW (green, 1:10000, *LI-COR*, 92532213, RRID:AB_2715510); donkey anti-goat IgG IR Dye 800 CW (green, 1:10000, *LI-COR*, 92532214, RRID:AB_2687553); donkey anti-mouse IgG IR Dye 800 CW (green, RRID:AB_2716622) and 680RD (red) (1:10000, *LI-COR*, 92532213, RRID:AB_2814912). The following secondary antibodies were used for immunohistochemistry; donkey anti-mouse Alexa

Fluor 647 (1:1000, Thermo Fisher Scientific, A31787, RRID:AB_2762830); goat anti-rabbit Alexa Fluor 488 (1:1000, Thermo Fisher Scientific, A11008, RRID:AB_143165); goat anti-chicken Alexa Fluor 488 (1:500, Thermo Fisher Scientific, A11039, RRID:AB_142924).

Transfection and viral transduction

Primary cultures of CGNs were transfected between 5 and 7 DIV with Lipofectamine 2000 using an established protocol.[44] In knockdown experiments, only the respective shRNA in the pSuper-mCer vector was transfected, whereas in rescue experiments, PI4KIIα-shRNA in pSuper mCer was co-expressed with shRNA resistant rescue constructs. For syp-pH experiments, syp-pH was co-transfected with either PI4KIIα-shRNA in the pSuper mCer vector, or the respective scrambled control. The one exception was a triple transfection in Figures 1K–1M, where syp-pH was co-transfected with PI4KIIα-shRNA and either shRNA resistant PI4KIIα or an empty vector control. In all cases, CGNs were imaged 3 days after transfection, equating to 8–10 DIV. For lentiviral transduction, CGNs were incubated with lentivirus expressing either PI4KIIα-shRNA or scrambled shRNA for 24 h at 1 DIV. Lentivirus-containing media was then replaced with conditioned media and CGNs were used at 9 DIV.

Lentiviral particle production and transduction

Lentiviral particles were produced as described.[79] HEK293T cells were transfected with three plasmids FUp95GW, psPAX2 and p-CMV-VSV-G (molar ratio 2:1:1) using Lipofectamine 2000. Cells were incubated with the DNA:Lipofectamine 2000 mixture for 8 h at 37°C before the FBS media was replaced with CGN culture media. The media containing viral particles was collected at day 3, filtered using 0.45 μm filter and used directly for transducing neuronal cultures on DIV 1.

Single cell TMR-dextran imaging

Transfected CGN cultures were removed from culture medium at DIV 8–10 and allowed to repolarize for 10 min in incubation medium (170 mM NaCl, 3.5 mM KCl, 0.4 mM KH_2PO_4, 20 mM TES [N-Tris-HCl (hydroxymethyl)-methyl-2-aminoethane sulfonic acid], 5 mM NaHCO3, 5 mM glucose, 1.2 mM Na_2SO_4, 1.2 mM $MgCl_2$, 1.3 mM $CaCl_2$, pH 7.4). Cultures were mounted in a Warner imaging chamber with embedded parallel platinum wires (RC-21BRFS). TMR-dextran solution (50 μM in incubation medium) was applied to the cells in the imaging chamber and the cells were challenged with a train of 400 field potentials at 40 Hz (100 mA, 1 ms pulse width). After stimulation, the cells were immediately washed and placed on the stage of either a Zeiss Axio Observer A1 or a Zeiss Axio Observer.Z1 epifluorescence microscope. Transfected neurons were visualized with either a Zeiss Plan Apochromat 40× oil immersion objective (NA 1.3) or a EC Plan-Neofluar 40× oil immersion objective (NA 1.3). Transfected neurons were visualised at 430 nm excitation (beam splitter 455 nm, emission 460–500 nm) and TMR-dextran labeling visualised at 550 nm (beam splitter 570 nm, emission 570–640 nm). For experiments using the Zeiss Axio Observer.Z1 microscope epifluorescence microscope excitation was provided by a Colibri 7 Solid-State Light Source.

Fluorescent images were captured using either a Zeiss AxioCam MRm Rev.3 or Zeiss AxioCam 506 digital camera and processed offline using FIJI 1.43 software (NIH). Neurite lengths were measured in the mCerulean channel using the Simple Neurite Tracer plugin. For quantification of TMR-dextran uptake, mCerulean and TMR-dextran images were overlaid using FIJI and the relevant puncta (those overlapping with the transfected neurite) were counted. If not indicated otherwise, n refers to the number of individual transfected neurons examined. For every condition in each preparation, one coverslip was incubated with TMR-dextran, but not stimulated to control for non-specific uptake. The number of TMR-dextran puncta from unstimulated neurons (if any) were subtracted from TMR-dextran puncta from stimulated coverslips.

TMR-dextran field imaging

CGNs were removed from culture medium at DIV 9 and transferred into basic incubation medium in presence of 30 μM of either PI4KII$\alpha_{26\text{-}58}$S47/51D, PI4KII$\alpha_{26\text{-}58}$S47/51A or PI4KII$\alpha_{26\text{-}58}$Scr peptide for 15 min. Cultures were then mounted in a Warner stimulation chamber in presence of 50 μM TMR-dextran and 30 μM of the respective peptide in incubation medium. Cultures were then immediately challenged with a 400 field potential train delivered at 40 Hz. After stimulation, the cells were immediately washed and placed on the stage of either a Zeiss Axio Observer A1 or a Zeiss Axio Observer.Z1 epifluorescence microscope and images were acquired using identical objectives and illumination to that for single cell TMR-dextran experiments. Experiments using PI-273 were performed in an identical manner with the exception that 1 μM PI-273 was incubated with CGNs in culture media for 48 h before TMR-dextran loading. PI-273 (1 μM) was also present prior to and during TMR-dextran loading.

At least five fields of comparable cell density were selected from each coverslip. The number of TMR-dextran puncta per field of view was determined using a self-written macro in FIJI. The macro uses the Maximum Entropy and Analyze Particles algorithms to threshold the image and count puncta between 0.3 and 2.5 μm. For each condition, a coverslip of cells was exposed to an identical treatment but minus stimulation (to control for background TMR-dextran uptake). These values were subtracted from stimulated values to provide a final activity-dependent uptake of TMR-dextran per field of view.

Morphological analysis of CGN nerve terminals

Lentivirus-transduced CGNs were removed from culture medium at DIV 9 and repolarized in incubation medium. After 10 min, CGNs were mounted into an RC-21BRFS stimulation chamber and challenged with 400 action potentials (40 Hz). Immediately following the

end of stimulation, cultures were fixed with a solution of 2% glutaraldehyde and 2% PFA in 0.1 M in phosphate buffer (PB). After washing in 0.1 M PB, cultures were stained with 1% osmium tetroxide for 30 min. Samples were then dehydrated using an ethanol series and polypropylene oxide and embedded using Durcupan resin. Samples were sectioned, mounted on grids, and viewed using an FEI Tecnai 12 transmission electron microscope (Oregon, USA). Intracellular structures that were <100 nm in diameter were arbitrarily designated to be SVs, whereas larger structures were considered endosomes. Typically, at least 10 fields of view were acquired for one coverslip of cells. The average number of endosomes and SVs per nerve terminal was calculated for each coverslip and represents the experimental n.

Syp-pH imaging

CGNs were removed from culture medium and repolarized in incubation medium as described above. CGNs expressing syp-pH were examined on a Zeiss Axio Observer A1 epifluorescence microscope using a Zeiss Plan Apochromat oil immersion objective (NA 1.3) at 500 nm using a 515 nm beamsplitter and emission 520–550 nm. Cultures were subjected to continuous perfusion with incubation medium and received a train of either 400 action potentials delivered at 40 Hz or 200 action potentials delivered at 20 Hz where indicated. For experiments examining Pr, CGNs were incubated with 1 mM bafilomycin A1 for 1 min before a 30 Hz (2 s) stimulus followed by a subsequent 30 Hz (45 s) stimulus. To reveal total pHluorin fluorescence, cultures were challenged with alkaline imaging buffer (50 mM NH_4Cl substituted for 50 mM NaCl) at the end of the experiment. Experiments examining both Pr and presynaptic performance (Figures 2H–2K) were performed on a Zeiss Axio Observer D1 epifluorescence microscope using a Zeiss EC Plan Neofluar oil immersion objective (NA 1.3) at 500 nm using a 515 nm beamsplitter and emission >520 nm. Fluorescent images were acquired at 4-s intervals using a Zeiss AxioCam MRm Rev.3 digital camera and processed offline using FIJI. Regions of interest of identical size were placed over nerve terminals, and the total fluorescence intensity was monitored over time. Only regions that responded to action potential stimulation were selected for analysis. Where required, traces were decay corrected using a mono-exponential decay function fitted to the first 15 points of acquisition. The pHluorin fluorescence change was calculated as $\Delta F/F_0$, and n refers to the number of individual coverslips examined.

Quantification of knockdown of PI4KIIα interaction partners

Opti-MEM was used to prepare a mixture of 2 μg shRNA for either AGAP2, CAMKV, BRSK1, STOP175 or TRIM3 or scrambled shRNA per well with 4 μL Lipofectamine 2000. The mixture was incubated at room temperature for 15 min and added dropwise to the culture medium of N2A cells. N2A cells were maintained at 37°C and 5% CO_2 for 72 h before lysis in SDS sample buffer (67 mM SDS, 2 mM EGTA, 9.3% glycerol, 12% β-mercaptoethanol, bromophenol blue, 67 mM Tris-HCl, pH 7.4). The lysates were vortexed and placed in an ultrasonicator for 5 min before boiling for 5 min at 95°. For analysis of knockdown efficiency, lysate was separated by SDS-PAGE and subjected to western blotting. Actin was blotted as a control for protein levels. Primary antibodies were used at double the concentration when compared to pull down experiments.

Immunofluorescence

CGNs between 8 and 10 DIV were removed from culture medium, left for 10 min in incubation medium and then fixed in 4% PFA in PBS solution for 20 min. Cells were washed with 50 mM NH_4Cl in PBS for 10 min and permeabilised in 0.1% Triton X-100 in PBS for 4 min twice. Cells were blocked with 1% BSA in PBS for 30 min at room temperature or overnight at 4°C. Cells were incubated with primary antibody (synaptotagmin-1, EGFP, FLAG, PI4KIIα or SV2A) for 1h at room temperature. Cells were washed with PBS three times, incubated with secondary antibody (Alexa Fluor 488 and -647, Thermo Scientific, Loughborough, UK) for the same time period at room temperature, before washing and mounting on slides using FluorSave (Merck, Kenilworth, USA). CGNs were imaged using an Axio Observer Z1 inverted epifluorescence microscope (Zeiss, Germany) with an EC Plan-Neofluar 40× oil immersion objective (NA 1.3) and Colibri 7 LED light source (Zeiss). Images of neurons were acquired in the green (exciter 450–490 nm, beam splitter 495 nm, emitter 500–550 nm), red (exciter 538–562 nm, beam splitter 570 nm, emitter 570–640 nm) and far-red (exciter 625–655 nm, beam splitter 660 nm, emitter 665–715 nm) range. Images were analyzed using the JaCoP-Plugin for FIJI, which displays Pearson's coefficient as a measure of the probability that a bouton that is positive for synaptotagmin-1 will also be positive for either PI4KIIα or SV2A. If not indicated otherwise, n numbers refers to the number of individual coverslips examined.

Quantification of PI4KIIα expression was performed in an identical manner, except coverslips were imaged on a Zeiss Axio Observer A1 epifluorescence microscope using a Zeiss Plan Apochromat oil immersion objective (NA 1.3). Transfected neurons (GFP) were visualised at 430-nm excitation (beam splitter 455 nm, emission 460–500 nm) with PI4KIIα visualised at 550 nm (beam splitter 570 nm, emission 570–640 nm). Images from each region were overlaid and regions of interest of identical sizes were placed over transfected synaptic boutons and the fluorescence in the PI4KIIα channel was quantified using FIJI with the Time Series analyser plugin. Equal-sized regions of interest were then placed over non-transfected synaptic boutons, with their fluorescence intensity quantified as above. Regions of interest of equal size were also placed over areas adjacent to synaptic boutons that were devoid of neurons, to acquire the average background fluorescence intensity. Background intensity was subtracted from both transfected and non-transfected fluorescence values. The average corrected transfected value was then expressed normalised to the non-transfected value, giving PI4KIIα expression as a percentage of non-transfected neurons. In all cases, n represents number of transfected CGNs imaged.

GST-fusion protein expression and affinity purification of nerve terminal proteins

Expression, induction and purification of GST-PI4KIIα N-term fusion proteins were performed as described.[10] The P2 synaptosome pellet was re-suspended in HEPES-buffered-Krebs (HBK, 118.5 mM NaCl, 4.7 mM KCl, 1.18 mM $MgSO_4$, 10 mM Glucose, 1 mM Na_2HPO_4 and 20 mM HEPES) and re-centrifuged at 20,200 *g* for 15 min. Synaptosomes were then lysed in ice-cold lysis buffer (1% Triton X-100, 150 mM NaCl, 25 mM Tris-HCl, 1 mM EDTA, 1 mM EGTA, 20 mg/mL leupeptin, 1 mM phenylmethylsulfonyl fluoride and protease inhibitor mix, pH 7.4) for 15 min and then centrifuged at 20,442 g for 5 min. Synaptosome lysates were incubated with GST fusion proteins which were previously coupled to GSH-Sepharose beads at 4°C for 2 h with rotation. The beads were washed extensively with ice-cold lysis buffer, lysis buffer containing 500 mM NaCl and finally twice with ice-cold 20 mM Tris-HCl buffer prior to heating for 5 min to 95°C in SDS sample buffer to facilitate elution of bound proteins.

Western blotting

Eluted GST-pull down samples were separated using SDS-PAGE and transferred to nitrocellulose membrane using a Bio-Rad Mini Trans-Blot Cell transfer apparatus. After staining with Ponceau S solution to reveal the GST fusion proteins, the membrane was incubated for 1 h in Intercept blocking buffer before overnight incubation rotating at 4°C in blocking buffer containing 0.1% Tween 20 and the respective primary antibody (see dilutions above). The membranes were washed three times for 10 min in washing buffer (PBS plus 0.1% Tween 20) before and after a 2 h incubation with secondary antibody (see dilutions above) under rotation. Fluorescence intensity was detected using the Licor-Odyssey fluorescent imaging system and Licor Image Studio Lite software (version 5.2). Quantification of binding to GST fusion proteins was performed using FIJI software. The extent of interactor binding was quantified as follows. For each repeat experiment, the density of interactor bands were normalised to the highest signal of each repeat. An identical approach was followed for Ponceau stains of GST fusion proteins on the same blot. The ratio of interactor to GST fusion protein values was calculated for each condition, to compensate to small differences in the amount of GST fusion protein present. Values were then normalised to the control condition (100%) dependent on the experiment performed. The n displayed refers to individual experiments.

In-gel digestion and LC MS identification of proteins

Coomassie stained gel slices were destained with 50% acetonitrile/50 mM ammonium bicarbonate solution and subsequently dehydrated with 100% acetonitrile. Proteins were digested using sequencing-grade modified trypsin (Promega) with overnight incubation at 37°C, and peptides were first extracted in 1% (v/v) formic acid/2% (v/v) acetonitrile followed by a second extraction in 50% (v/v) acetonitrile. The extracts were combined and the resulting digested peptides were cleaned up using Stagetips by following standard protocol.[80]

NanoflowLC-MS/MS was performed on a micrOTOF-II mass spectrometer (Bruker, Germany) coupled to a RSLCnano LC system (Thermo) following an earlier method.[81] Raw spectral data were processed with DataAnalysis (Bruker) software and the resulting peak lists were searched using Mascot 2.4 server (Matrix Science) against Uniprot rat sequence database containing 35,737 entries. Mass tolerance on peptide precursor ions was fixed at 25 ppm and on fragment ions at 0.05 Da. Trypsin specificity was used allowing up to one missed cleavage. The peptide charge was set to 2+ and 3+ and oxidation of methionine and de-amidation were chosen as variable modifications.

QUANTIFICATION AND STATISTICAL ANALYSIS

Statistical analysis was performed using GraphPad Prism 8.4.3. No statistical methods were used to predetermine sample sizes. Randomization and blinding was applied to coverslips prior to fluorescence imaging and analysis. Statistical tests were applied based on the distribution of the datasets measured using D'Agostino-Pearson normality test. All data is presented as mean ± standard error of the mean, with significance set at ns $p > 0.05$, *$p < 0.05$, **$p < 0.01$, ***$p < 0.001$, **** $p < 0.0001$. Mann-Whitney (two-tailed) tests were used to compare non-Gaussian datasets. Student's t test (two-tailed) and analyses of variance (ANOVA) followed by Dunnett's post-hoc test were used to compare normally distributed datasets. All statistical information is provided in Table S2.

Cell Reports, Volume *42*

Supplemental information

Phosphatidylinositol 4-kinase IIα is a glycogen synthase kinase 3-regulated interaction hub for activity-dependent bulk endocytosis

Eva-Maria Blumrich, Jessica C. Nicholson-Fish, Marie Pronot, Elizabeth C. Davenport, Dominic Kurian, Adam Cole, Karen J. Smillie, and Michael A. Cousin

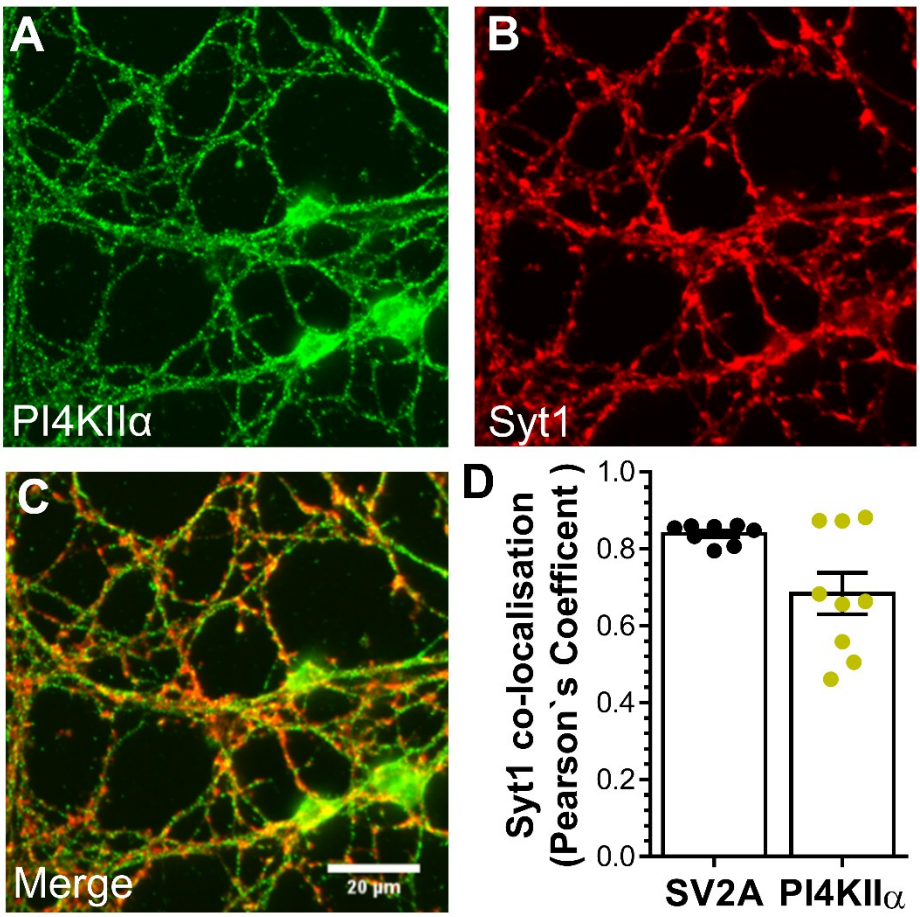

Figure S1 - *PI4KIIα is located at central nerve terminals, related to Figure 1.* Primary cultures of CGNs between 8-10 DIV were fixed and immunostained for synaptotagmin-1 (Syt1) and either PI4KIIα or SV2A. Representative images display PI4KIIα (**A**) or Syt1 (**B**) staining and a merged image (PI4KIIα green, Syt1 red, **C**). Scale bar = 20 µm. (**D**) Quantification of co-localisation with Syt1 for either SV2A or PI4KIIα ± SEM (Syt1/ PI4KIIα, n=9, Syt1/SV2A n=8).

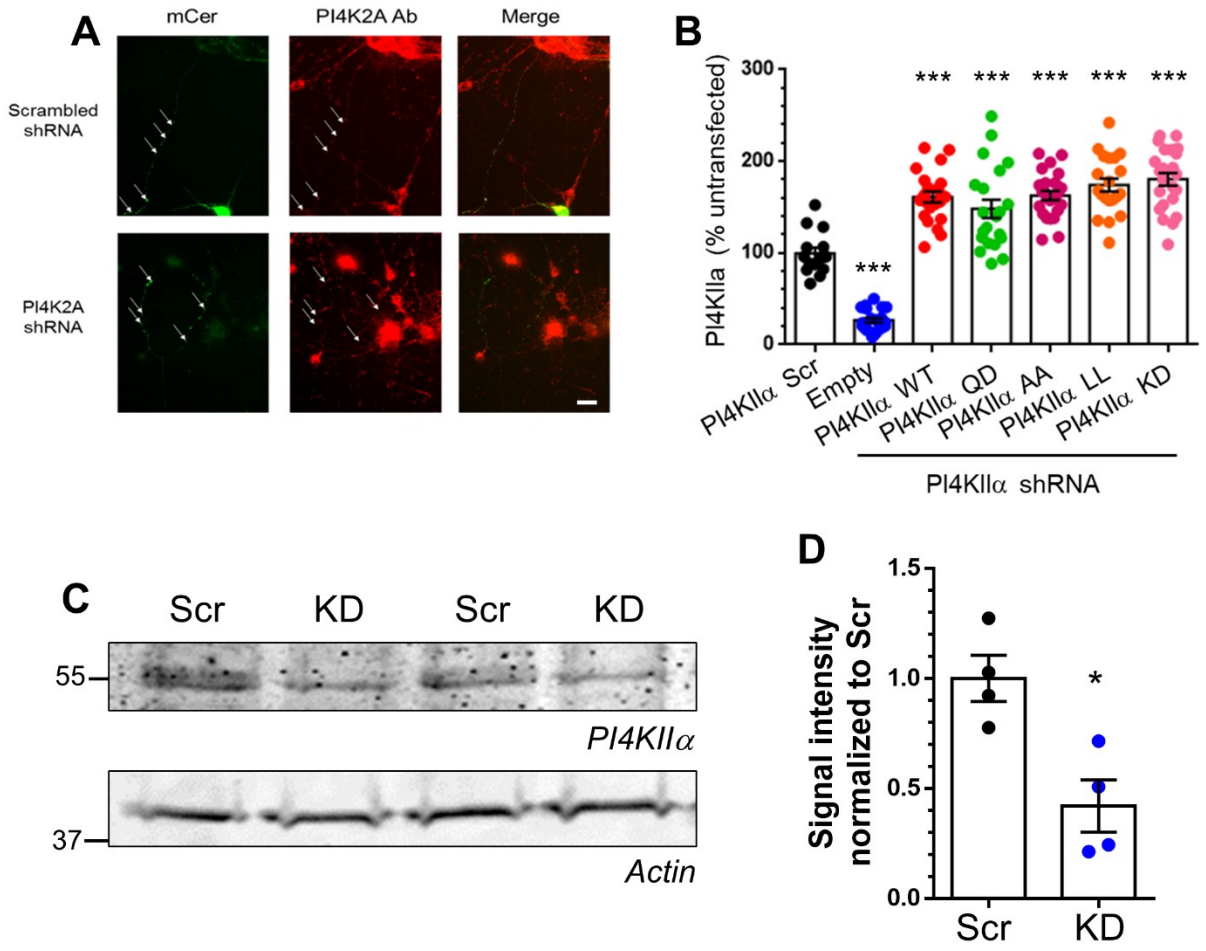

Figure S2 – *Expression of endogenous and exogenous PI4KIIα, related to Figures 2 and 3.* (**A,B**) Primary cultures of CGNs between 5-7 DIV were transfected with shRNA against PI4KIIα or a scrambled control (Scr). CGNs expressing PI4KIIα shRNA were co-transfected with either FLAG-tagged versions of PI4KIIα (WT), PI4KIIα-QD, PI4KIIα-S9/51A, PI4KIIα-L60/61A, PI4KIIα-K152A or a FLAG-empty vector (Emp). At 8-10 DIV, CGNs were fixed and immunostained for PI4KIIα. (**A**) Representative images are displayed for CGNs expressing either Scr or PI4KIIα shRNA. Scale bar = 10 μm. (**B**) Quantification of PI4KIIα expression ± SEM (Scr n=14, Emp, WT, QD n=21, S9/51A n=25, L60/61A n=20, K152A n=25, ****p<0.0001, one-way ANOVA against Scr, Dunnett's multiple comparison test. (**C,D**) CGNs were transduced with lentivirus expressing either shRNA against PI4KIIα (KD) or a scrambled control (Scr) on DIV 1. CGNs were lysed on DIV 9 and the presence of PI4KIIα was assessed by western blotting. (**C**) Representative blot of PI4KIIα in Scr and KD samples, with actin used as a loading control. (**D**) Quantification of PI4KIIα levels normalised to actin and then the Scr control ± SEM (both n=4, * p=0.0286, Mann-Whitney test).

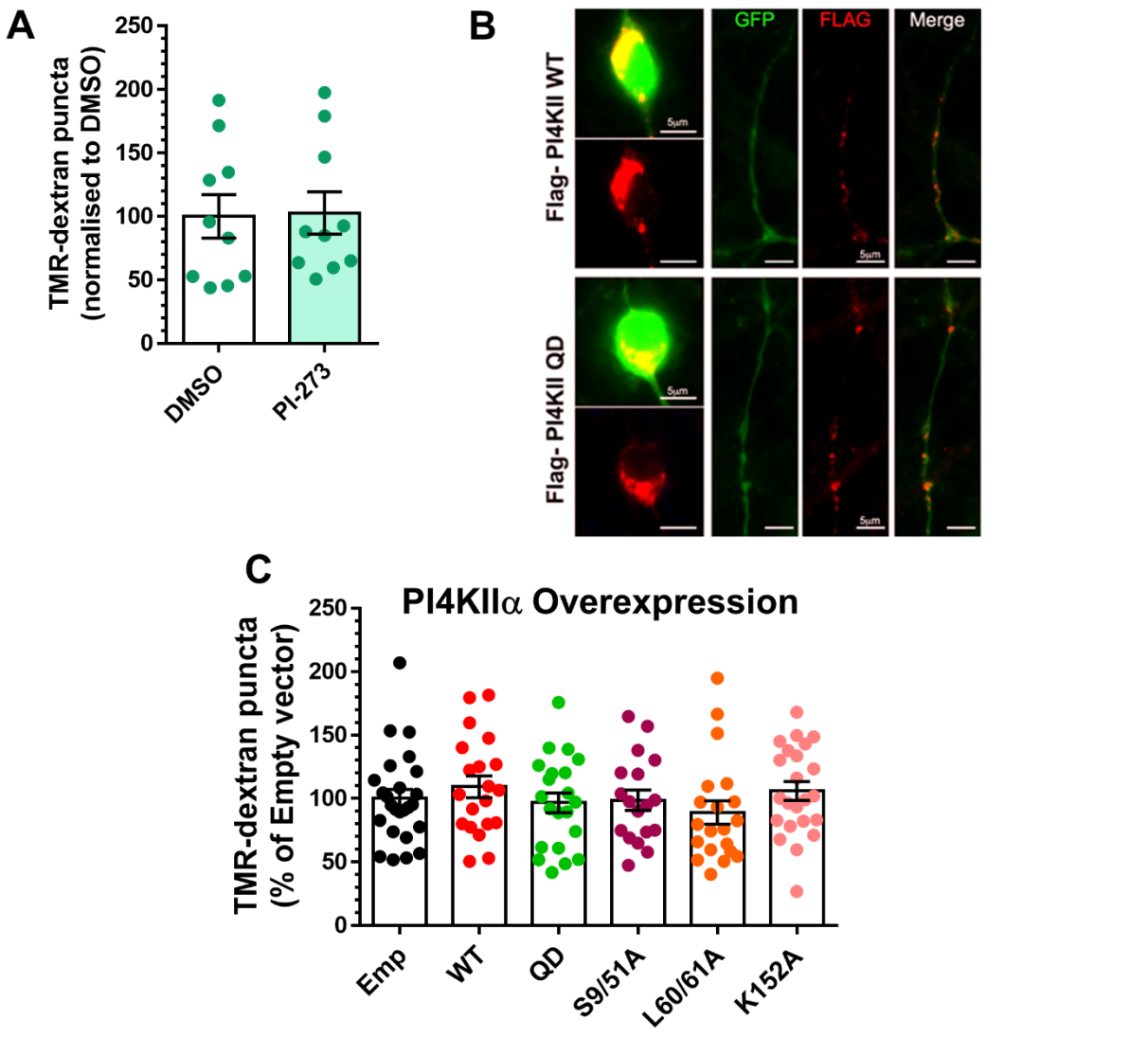

Figure S3 – *Inhibition of PI4KIIα activity or overexpression of PI4KIIα mutants does not affect ADBE, related to Figure 3*. (**A**) Primary cultures of CGNs were incubated for 48 hours in the presence of 1 μM PI-273 or a vehicle control (DMSO). In the continued presence of 1 μM PI-273 or DMSO, CGNs were stimulated with a train of 400 action potentials (40 Hz) in the presence of 50 μM TMR-dextran for 2 min. TMR-dextran was then immediately washed away and images acquired. Mean TMR-dextran uptake is presented as a proportion of DMSO uptake ± SEM (both n=10, students t test, p=0.909). (**B**) Primary cultures of CGNs were transfected with GFP and either FLAG-tagged versions of either PI4KIIα (WT) or PI4KIIα-QD between 5-7 DIV. At 8-10 DIV, CGNs were fixed and immunostained for the presence of GFP (green) and FLAG (red). Left hand panels display the TGN localisation of PI4KIIα as either a merged or FLAG image. Right hand panels display the localisation of WT and QD PI4KIIα at nerve terminals. Scale bar 5 μm for all images. (**C**) Primary cultures of CGNs were transfected with FLAG-tagged versions of PI4KIIα (WT), PI4KIIα-QD, PI4KIIα-S9/51A, PI4KIIα-L60/61A, PI4KIIα-K152A or a FLAG-empty vector (Emp) between 5-7 DIV. At 8-10 DIV, CGNs were stimulated with a train of 400 action potentials (40 Hz) in the presence of 50 μM TMR-dextran for 2 min. Mean TMR-dextran uptake as a proportion of uptake in Emp expressing CGNs ± SEM (Emp n=25, WT, L60/61A n=20, QD n=21, S9/51A n=18, K152A n=23, all ns, one-way ANOVA against Emp.

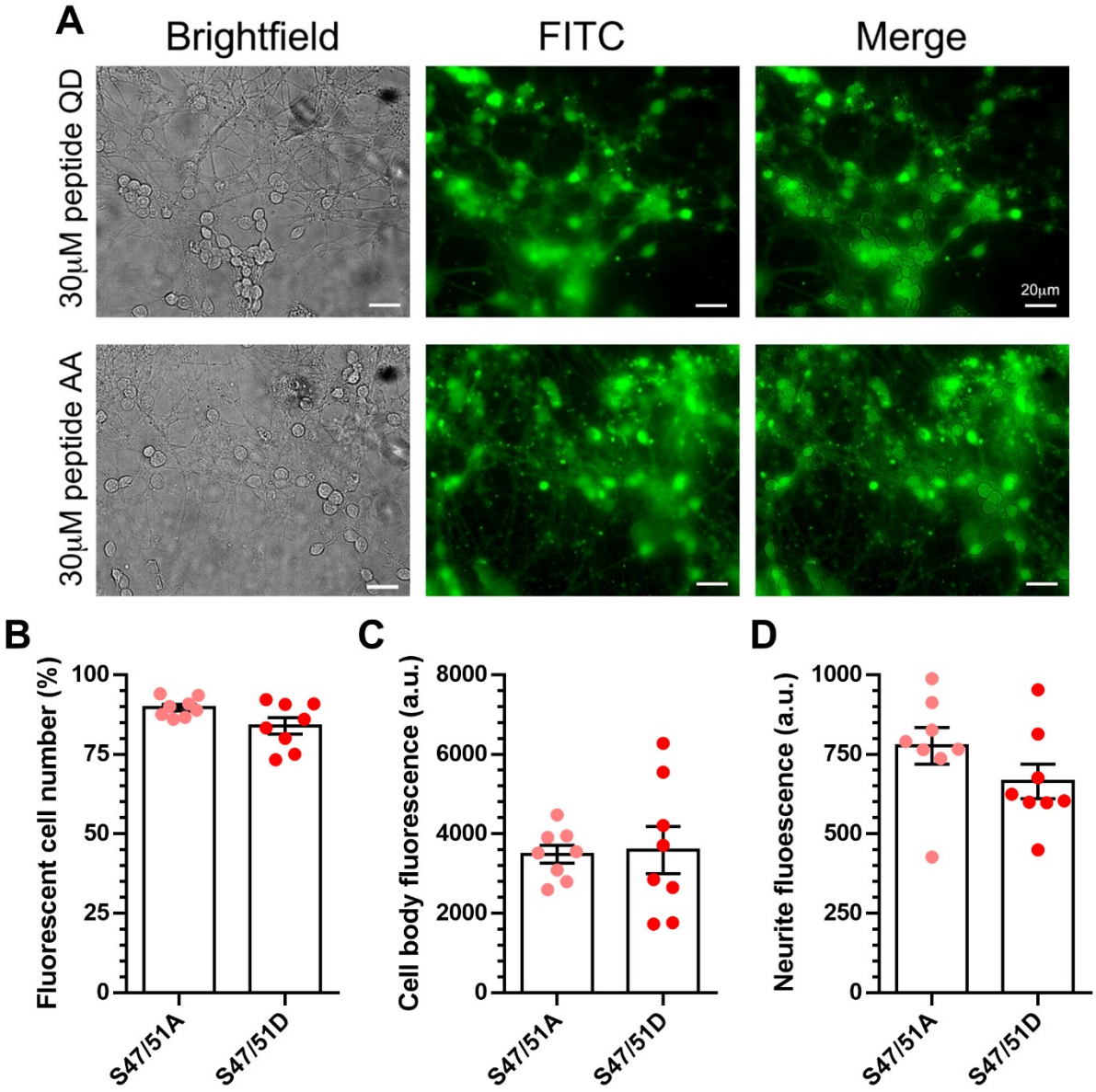

Figure S4 – *Equal entry of PI4KIIα$_{26-58}$S47/51A and PI4KIIα$_{26-58}$S47/51D peptides into CGNs, related to Figure 5.* Primary cultures of CGNs (DIV 9) were removed from culture medium at and transferred into basic incubation medium in presence of 30 µM of either FITC-PI4KIIα$_{26-58}$S47/51D or FITC-PI4KIIα$_{26-58}$S47/51A peptides for 15 min. (**A**) Representative images of a typical field when viewed using bright field (left), in the FITC channel (middle) and a merged image (right). (**B-D**) Quantification (all ± SEM) of peptide uptake expressed as either, percentage of fluorescent cell bodies per field of view (**B**), fluorescence intensity at cell bodies (**C**) or neurites (**D**). For all experiments n = 8 fields of view for both FITC-PI4KIIα$_{26-58}$S47/51D and FITC-PI4KIIα$_{26-58}$S47/51A peptides (all ns, Mann-Whitney test, **B** p = 0.123, **C** p = 0.932, **D** p = 0.159).

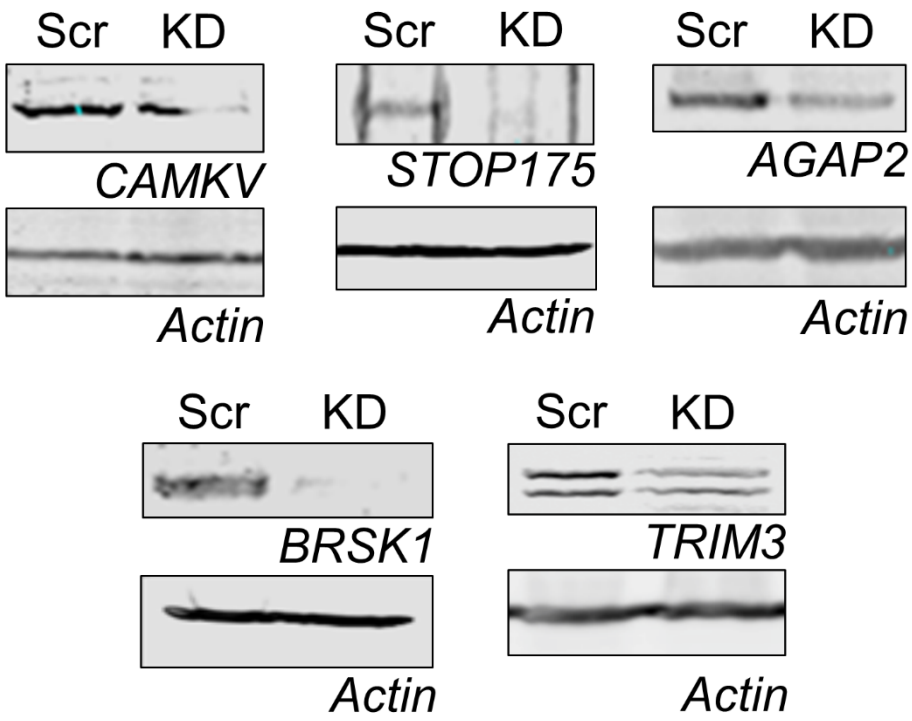

Figure S5 – *Knockdown of phospho-dependent PI4KIIα interaction partners, related to Figure 7*. Cultures of N2A cells were transfected with shRNA against either CAMKV, AGAP2, BRSK1, TRIM3, STOP175 or a control scrambled sequence (Scr). After 48 hours N2A cells were lysed and blotted for the presence of CAMKV, AGAP2, BRSK1, TRIM3 or STOP175. Actin blots from the same lysate samples are also displayed.

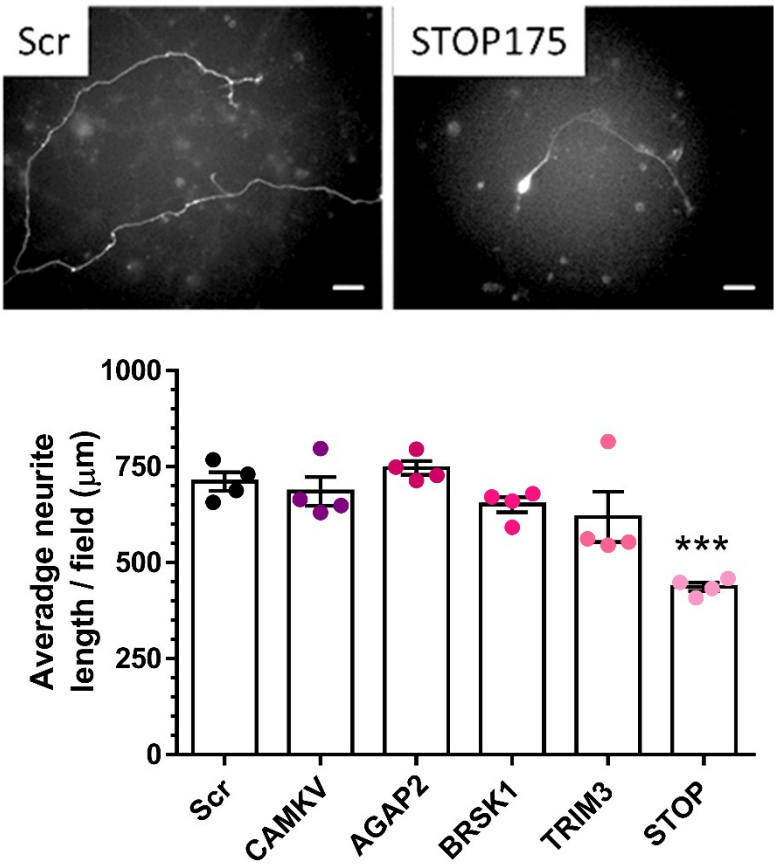

Figure S6 – *Quantification of effects on axon outgrowth during knockdown of phospho-dependent PI4KIIα interaction partners, related to Figure 7*. Primary cultures of CGNs were transfected with shRNA against either AGAP2, BRSK1, CAMKV, TRIM3, STOP175 or a scrambled (Scr) control. Representative images for CGNs transfected with either Scr or STOP175 are displayed. Scale bar is equivalent to 30 μm. Quantification of axon length was performed using the Neurite-Tracer-Plugin in FIJI, by analysing images of transfected neurons from TMR-dextran uptake experiments (Figure 6). All neurites of transfected CGNs were counted and measured by opening the image in the Neurite-Tracer and following its path. The plugin uses the metadata of the image to convert the measured pixels into micrometers, from which the average length per neurite was calculated. Bar graph displays the mean average axon length ± SEM all conditions (all n = 4 coverslips).

Protein	Alternative names	Reported / potential involvement in SV trafficking or recycling
AGAP2	PIKE-A Centaurin-γ1A	ArfGAP function, activator Arf GTPases[49]
		Endolysosomal cargo sorting via AP-1 interactions and Arf1 regulation[48,50]
		Recycling of β-adrenergic receptors via ERK interactions[51]
		Control of postsynaptic AMPA receptor surface expression[68]
BRSK1	SAB-D	Localised to SVs and active zone, negative regulator of neurotransmitter release[52]
		Control of RRP replenishment via CAST phosphorylation[53]
STOP-175	Microtubule stabilizing Protein 6 (MAP-6)	Binds and stabilizes microtubules in neurons[58]
		Interacts with guidance molecule to drive axonal development[59]
		Palmitoylation-dependent recruitment to define the axonal compartment[60]
TRIM3		Ubiquitin E3 ligase, modulator of motor protein KIF21B[57]
		Control of synaptic γ-actin turnover and hippocampal synaptic plasticity[56]
CAMKV		Calmodulin-binding pseudokinase, enriched on SVs[55]
		A cdk5 substrate, required for spine maintenance and hippocampal synaptic plasticity[54]

Table S1: Overview of reported functions related to vesicle trafficking and transport of the five proteins showing enhanced binding to the PI4KIIα-QD mutant.

Figure 1	Group	Mean±SEM	n = # of coverslips/ N = # of neuronal preparations	Comparison	P	Statistical test
1F	Scr	5.8 ± 0.8 %	11/3	Scr vs KD	0.791	Mann-Whitney test
	KD	6.2 ± 1.3 %	7/3			
1G	Scr	26.1 ± 2.6 s	11/3	Scr vs KD	0.285	Mann-Whitney test
	KD	21.7 ± 2.2 s	7/3			
1I	Scr	27.5 ± 2.5 %	13/3	Scr vs KD	0.130	Unpaired t-test
	KD	21.2 ± 3.1 %	13/3			
1J	Scr	37.3 ± 3.9 s	13/3	Scr vs KD	0.004	Unpaired t-test
	KD	24.1 ± 1.4 s	13/3			
1L	KD	34.3 ± 4.0 %	12/3	KD vs Rescue	0.055	Unpaired t-test
	Rescue	44.8 ± 2.6 %	9/3			
1M	KD	29.2 ± 3.4 s	12/3	KD vs Rescue	0.013	Unpaired t-test
	Rescue	44.8 ± 3.7 s	9/3			

Figure 2	Group	Mean±SEM	n = # of coverslips/ N = # of neuronal preparations	Comparison	P	Statistical test
2C	Scr	100.0 ± 14.5 %	8/3	Scr vs KD	0.0037	Mann-Whitney test
	KD	43.9 ± 5.7 %	7/3			
2F	Scr	24.65 ± 1.36	4/2	Scr vs KD	0.2452	Unpaired t-test
	KD	21.31 ± 2.35	3/2			
2G	Scr	4.105 ± 0.244	4/2	Scr vs KD	0.0009	Unpaired t-test
	KD	1.558 ± 0.257	3/2			
2I	Scr	0.323 ± 0.080	5/2	Scr vs KD	0.9096	Unpaired t-test
	KD	0.311 ± 0.052	5/4			
2K	Scr		6/4	Scr vs KD	0.0057	Two-way ANOVA
	KD		6/4			
	Scr Stim 1	1.0 ± 0.0	6/4	Scr vs KD	>0.9999	Two-way ANOVA with Sidak's multiple comparison test
	KD Stim 1	1.0 ± 0.0	6/4			
	Scr Stim 2	0.955 ± 0.065	6/4	Scr vs KD	0.9998	
	KD Stim 2	0.941 ± 0.069	6/4			
	Scr Stim 3	1.028 ± 0.069	6/4	Scr vs KD	0.0075	
	KD Stim 3	0.716 ± 0.069	6/4			
	Scr Stim 4	0.963 ± 0.087	6/4	Scr vs KD	0.0004	
	KD Stim 4	0.561 ± 0.094	6/4			

Figure 3	Group	Mean±SEM	n = # experiments	Comparison	P	Statistical test
3G	Emp	45.5 ± 4.3 %	32/4	Emp vs all	<0.0001	One-way ANOVA with Dunnett's multiple
	WT	100 ± 7.1 %	25/4			
	QD	56.7 ± 9.5 %	13/4		ns	
	S9/51A	84.6 ± 6.5 %	32/4		<0.0001	

	L60/61A	83.1 ± 4.3 %	32/4		<0.0001	comparison test
	K152A	93.6 ± 5.8 %	30/4		<0.0001	
Figure 4	Group	Mean±SEM	n = # experiments	Comparison	P	Statistical test
4B	WT	1.00 ± 0.19	5	BRSK WT vs all	0.0026	One-way ANOVA with Dunnett's multiple comparison test
	QD	2.38 ± 0.27	5			
	S9/51A	1.34 ± 0.31	5		0.6438	
	L60/61A	1.02 ± 0.14	5		0.9999	
4C	WT	1.22 ± 0.18	7	CAMKV WT vs all	0.0111	
	QD	2.71 ± 0.49	7			
	S9/51A	1.55 ± 0.37	7		0.8223	
	L60/61A	0.98 ± 0.16	7		0.9205	
4D	WT	0.39 ± 0.09	4	AGAP2 WT vs all	0.0001	
	QD	1.46 ± 0.16	4			
	S9/51A	0.39 ± 0.05	4		>0.9999	
	L60/61A	0.42 ± 0.14	4		0.9946	
4E	WT	0.49 ± 0.13	3	TRIM3 WT vs all	0.010	
	QD	1.35 ± 0.18	3			
	S9/51A	0.68 ± 0.16	3		0.7094	
	L60/61A	0.61 ± 0.16	3		0.8840	
4F	WT	0.58 ± 0.08	5	STOP175 WT vs all	0.0034	
	QD	1.63 ± 0.30	5			
	S9/51A	0.40 ± 0.17	5		0.8427	
	L60/61A	0.44 ± 0.15	5		0.9119	
Figure 5	Group	Mean±SEM	n = # experiments or n = # of coverslips/ N = # of neuronal preparations	Comparison	P	Statistical test
5C	FL	1.52 ± 0.12	4	BRSK FL vs all	0.2107	One-way ANOVA with Dunnett's multiple comparison test
	QD 58	0.78 ± 0.24	4			
	QD 24	0.03 ± 0.03	4		0.0017	
	FL	1.48 ± 0.14	4	CAMKV FL vs all	0.2555	
	QD 58	1.04 ± 0.17	4			
	QD 24	0.02 ± 0.02	4		0.0027	
	FL	1.02 ± 0.19	3	AGAP2 FL vs all	0.1377	
	QD 58	0.59 ± 0.16	3			
	QD 24	0.06 ± 0.06	3		0.0495	
	FL	1.40 ± 0.05	4	TRIM3 FL vs all	0.3647	
	QD 58	1,10 ± 0.18	4			
	QD 24	0.15 ± 0.10	4		0.0005	
	FL	0.95 ± 0.27	4	STOP175 FL vs all	0.3544	
	QD 58	0.81 ± 0.20	4			
	QD 24	0.33 ± 0.14	4		0.0630	
5E	Scr	100.0 ± 9.6	11/4	Scr vs. S47/51A	0.4668	
	S47/51A	82.2 ± 16.8	11/4	Scr vs. S47/51D	0.0007	
	S47/51D	30.7 ± 5.8	10/4	S47/51A vs. S47/51D	0.0100	

Figure 6	Group	Mean±SEM	n = # of coverslips/ N = # of neuronal preparations	Comparison	P	Statistical test
6C	WT	1.20 ± 0.14	6	BRSK WT vs all	0.0156	One-way ANOVA with Dunnett's multiple comparison test
	S47/51D	2.08 ± 0.30	6			
	S5/9D	0.96 ± 0.12	6		0.6366	
	WT	1.48 ± 0.11	6	CAMKV WT vs all	0.0079	
	S47/51D	2.21 ± 0.23	6			
	S5/9D	1.15 ± 0.09	6		0.2607	
	WT	0.67 ± 0.10	6	AGAP2 WT vs all	0.0045	
	S47/51D	1.50 ± 0.24	6			
	S5/9D	0.53 ± 0.11	6		0.7726	
	WT	0.76 ± 0.10	6	TRIM3 WT vs all	0.0003	
	S47/51D	1.89 ± 0.19	6			
	S5/9D	0.53 ± 0.17	6		0.5013	
	WT	0.70 ± 0.07	6	STOP175 WT vs all	0.0012	
	S47/51D	1.56 ± 0.22	6			
	S5/9D	0.59 ± 0.08	6		0.7846	
6E	Scr	100.0 ± 6.8 %	11/3	Scr vs all	<0.0001	One-way ANOVA with Dunnett's multiple comparison test
	Emp	53.92 ± 4.8 %	12/3			
	WT	85.6 ± 8.4 %	12/3		0.2403	
	QD	41.5 ± 3.3 %	12/3		<0.0001	
	S47/51D	43.9 ± 3.4 %	12/3		<0.0001	

Figure 7	Group	Mean±SEM	n = # coverslips/ N = # of neuronal preparations	Comparison	P	Statistical test
7G	Scr	100.0 ± 8.0 %	12/3	Scr vs all	<0.001	One-way ANOVA with Dunnett's multiple comparison test
	CAMKV	45.2 ± 5.7 %	9/3			
	AGAP2	28.0 ± 5.3 %	9/3		<0.0001	
	BRSK1	69.6 ± 11.6 %	9/3		0.0636	
	TRIM3	81.0 ± 8.5 %	9/3		0.321	
	STOP175	73.2 ± 19.8 %	5/3		0.2537	

Figure S1	Group	Mean±SEM	n = # of coverslips/ N = # of neuronal preparations	Comparison	P	Statistical test
S1	SV2A	0.84 ± 0.01	8/3	No comparison		
	PI4KIIα	0.68 ± 0.05	9/3			

Figure S2	Group	Mean±SEM	n = # of coverslips/ N = # of neuronal preparations	Comparison	P	Statistical test
S2B	Scr	1.0 ± 0.11	4/2	Scr vs KD	0.0286	Mann-Whitney test
	KD	0.42 ± 0.12	4/2			
S2D	Scr	100.0 ± 6.4 %	14/3	Scr vs all	<0.0001	

	Emp	26.8 ± 2.5 %	21/3			One-way ANOVA with Dunnett's multiple comparison test
	WT	163.7 ± 6.0 %	21/3		<0.0001	
	QD	148.8 ± 10.0 %	21/3		<0.0001	
	S9/51A	163.4 ± 4.9 %	25/3		<0.0001	
	L60/61A	175.0 ± 7.3 %	20/3		<0.0001	
	K152A	181.3 ± 7.0%	23/3		<0.0001	
Figure S3	Group	Mean±SEM	n = # of coverslips/ N = # of neuronal preparations	Comparison	P	Statistical test
S3A	DMSO	100.0 ± 17.1 %	10/3	DMSO vs PI-273	0.909	Unpaired t-test
	PI-273	102.8 ± 16.6 %	10/3			
S3C	Emp	100.0 ± 7.2 %	25/3	Emp vs all	0.8682	One-way ANOVA with Dunnett's multiple comparison test
	WT	109.3 ± 8.6 %	20/3			
	QD	96.7 ± 7.9 %	21/3		0.9982	
	S9/51A	98.7 ± 8.0 %	18/3		0.999	
	L60/61A	89.0 ± 9.2 %	20/3		0.7768	
	K152A	106.0 ± 7.3 %	23/3		0.9706	
Figure S4	Group	Mean±SEM	n = # of fields / N = # of coverslips	Comparison	P	Statistical test
S4B	S47/51A	89.7 ± 1.1	8/2	S47/51A vs. S47/51D	0.123	Mann-Whitney test
	S47/51D	83.9 ± 2.6	8/2			
S4C	S47/51A	3485 ± 223	8/2	S47/51A vs. S47/51D	0.932	
	S47/51D	3591 ± 593	8/2			
S4D	S47/51A	776.7 ± 58.2	8/2	S47/51A vs. S47/51D	0.159	
	S47/51D	664.7 ± 54.4	8/2			
Figure S6	Group	Mean±SEM	n = # of coverslips	Comparison	P	Statistical test
S6	Scr	710.9 ± 24.2	4	Scr vs CAMKV	0.9999	One-way ANOVA with Bonferroni's Multiple Comparison Test
	CAMKV	685.3 ± 37.8	4			
	AGAP2	746.4 ± 17.8	4	Scr vs AGAP2	0.9999	
	BRSK1	680.9 ± 19.9	4	Scr vs BRSK1	0.9999	
	TRIM3	619.1 ± 65.4	4	Scr vs TRIM3	0.3788	
	STOP175	437.3 ± 11.0	4	Scr vs STOP175	0.0001	

Table S2 – *Collated table of experimental n, P values and statistical tests, related to all Figures*.

Reference List

48. Nie, Z., Fei, J., Premont, R.T., and Randazzo, P.A. (2005). The Arf GAPs AGAP1 and AGAP2 distinguish between the adaptor protein complexes AP-1 and AP-3. Journal of cell science *118*, 3555-3566. 10.1242/jcs.02486.
49. Nie, Z., and Randazzo, P.A. (2006). Arf GAPs and membrane traffic. Journal of cell science *119*, 1203-1211. 10.1242/jcs.02924.
50. Shiba, Y., Römer, W., Mardones, G.A., Burgos, P.V., Lamaze, C., and Johannes, L. (2010). AGAP2 regulates retrograde transport between early endosomes and the TGN. Journal of cell science *123*, 2381-2390. 10.1242/jcs.057778.
51. Wu, Y., Zhao, Y., Ma, X., Zhu, Y., Patel, J., and Nie, Z. (2013). The Arf GAP AGAP2 interacts with β-arrestin2 and regulates β2-adrenergic receptor recycling and ERK activation. Biochem J *452*, 411-421. 10.1042/bj20121004.
52. Inoue, E., Mochida, S., Takagi, H., Higa, S., Deguchi-Tawarada, M., Takao-Rikitsu, E., Inoue, M., Yao, I., Takeuchi, K., Kitajima, I., et al. (2006). SAD: a presynaptic kinase associated with synaptic vesicles and the active zone cytomatrix that regulates neurotransmitter release. Neuron *50*, 261-275. 10.1016/j.neuron.2006.03.018.
53. Mochida, S., Hida, Y., Tanifuji, S., Hagiwara, A., Hamada, S., Abe, M., Ma, H., Yasumura, M., Kitajima, I., Sakimura, K., and Ohtsuka, T. (2016). SAD-B Phosphorylation of CAST Controls Active Zone Vesicle Recycling for Synaptic Depression. Cell reports *16*, 2901-2913. 10.1016/j.celrep.2016.08.020.
54. Liang, Z., Zhan, Y., Shen, Y., Wong, C.C., Yates, J.R., 3rd, Plattner, F., Lai, K.O., and Ip, N.Y. (2016). The pseudokinase CaMKv is required for the activity-dependent maintenance of dendritic spines. Nature communications *7*, 13282. 10.1038/ncomms13282.
55. Godbout, M., Erlander, M.G., Hasel, K.W., Danielson, P.E., Wong, K.K., Battenberg, E.L., Foye, P.E., Bloom, F.E., and Sutcliffe, J.G. (1994). 1G5: a calmodulin-binding, vesicle-associated, protein kinase-like protein enriched in forebrain neurites. The Journal of neuroscience : the official journal of the Society for Neuroscience *14*, 1-13. 10.1523/jneurosci.14-01-00001.1994.
56. Schreiber, J., Végh, M.J., Dawitz, J., Kroon, T., Loos, M., Labonté, D., Li, K.W., Van Nierop, P., Van Diepen, M.T., De Zeeuw, C.I., et al. (2015). Ubiquitin ligase TRIM3 controls hippocampal plasticity and learning by regulating synaptic γ-actin levels. The Journal of cell biology *211*, 569-586. 10.1083/jcb.201506048.
57. Labonté, D., Thies, E., Pechmann, Y., Groffen, A.J., Verhage, M., Smit, A.B., van Kesteren, R.E., and Kneussel, M. (2013). TRIM3 regulates the motility of the kinesin motor protein KIF21B. PloS one *8*, e75603. 10.1371/journal.pone.0075603.
58. Guillaud, L., Bosc, C., Fourest-Lieuvin, A., Denarier, E., Pirollet, F., Lafanechère, L., and Job, D. (1998). STOP proteins are responsible for the high degree of microtubule stabilization observed in neuronal cells. The Journal of cell biology *142*, 167-179. 10.1083/jcb.142.1.167.
59. Deloulme, J.C., Gory-Fauré, S., Mauconduit, F., Chauvet, S., Jonckheere, J., Boulan, B., Mire, E., Xue, J., Jany, M., Maucler, C., et al. (2015). Microtubule-associated protein 6 mediates neuronal connectivity through Semaphorin 3E-dependent signalling for axonal growth. Nature communications *6*, 7246. 10.1038/ncomms8246.
60. Tortosa, E., Adolfs, Y., Fukata, M., Pasterkamp, R.J., Kapitein, L.C., and Hoogenraad, C.C. (2017). Dynamic Palmitoylation Targets MAP6 to the Axon to Promote Microtubule Stabilization during Neuronal Polarization. Neuron *94*, 809-825.e807. 10.1016/j.neuron.2017.04.042.
68. Chan, C.B., Chen, Y., Liu, X., Tang, X., Lee, C.W., Mei, L., and Ye, K. (2011). PIKE-mediated PI3-kinase activity is required for AMPA receptor surface expression. EMBO J *30*, 4274-4286. 10.1038/emboj.2011.281.